

Finite temperature quantum noise correlations as a probe for topological helical edge modes

Sachiraj Mishra and Colin Benjamin*

School of Physical Sciences, National Institute of Science Education and Research, HBNI, Jatni-752050, India, and Homi Bhabha National Institute, Training School Complex, AnushaktiNagar, Mumbai, 400094, India .

The distinction between chiral, trivial helical, and topological helical edge modes can be effectively made using quantum noise measurements at finite temperatures. The use of quantum noise, both the cross (or the Hanbury-Brown Twiss) correlation and the autocorrelation can differentiate between these edge modes via the two contributions: thermal-like noise from thermal fluctuations and shot noise from the quantum nature of charge particles. The study of these edge modes at finite temperatures is important as it more accurately reflects the conditions in real-world experiments.

I. INTRODUCTION

The discovery of the integer quantum Hall effect[1] and the subsequent development of the Landauer-Buttiker formula[2],[3] were critical milestones in our understanding of electron transport in 2DEGs. The concept of chiral edge modes, which are responsible for quantized Hall resistance, has since been extended to other systems, including the quantum spin Hall(QSH) effect in materials such as HgTe/CdTe heterostructures[5], wherein edge modes are helical. The discovery of the QSH effect[6] was important because it demonstrated that spin-orbit scattering could be used to control the direction of spin polarization in edge modes, opening up new avenues for spintronics and quantum computing.

Chiral and helical edge modes are topologically protected and are not affected by the presence of impurities along the edge channels[2],[3]. Helical and chiral edge states can be distinguished by different methods, such as a conductance test using the Landauer-Buttiker approach[7]. However, a recent experiment showed that the helical edge states may not always be topologically protected[8]; instead, trivial helical edge modes can arise. In this case, it is essential to distinguish between the different kinds of helical edge states, a topological one and another non-topological or trivial. Of course, we can do a conductance measurement using the Landauer-Buttiker approach, but this cannot effectively show any distinction between trivial and topological helical edge modes[9]. In this case, it is wiser to rely upon the noise correlations[10], which can also be performed experimentally.

At zero temperature in a multiterminal conductor and in the presence of inelastic scattering, transport via chiral and helical edge modes can be distinguished via the non-local charge shot noise “HBT” correlations. For the transport via chiral edge modes, “HBT” correlations are always negative, while it is positive for transport via topological helical edge states[9]. The most significant advantage is that this quantity works as a probe for helicity because it turns negative for trivial helical edge

modes due to spin-flip scattering in the presence of inelastic scattering[9]. In addition, calculating the non-local shot noise correlation could successfully show distinct outcomes for different quantum transport schemes, such as via ballistic and trivial helical edge modes. It implies that experiments involving non-local shot noise can be instrumental in distinguishing different modes of quantum transport. However, this work has certain limitations. Firstly, this was at zero temperature, where only shot noise matters. Secondly, this does not distinguish between the trivial and topological helical edge modes for low spin-flip probabilities, which is a disadvantage for experiments in clean samples where spin-flip scattering is low. Thirdly, this setup does not provide any information regarding the distinction via shot noise autocorrelation. In this work, we remove these limitations by showing the differentiation between the chiral and topological helical edge modes and between the helical trivial and topological edge modes for any arbitrary value of spin-flip scattering by studying both cross and autocorrelation of the quantum noise at finite temperatures.

One can perform the noise experiment at very low temperatures, such as 50nK and 10mK, as reported in QSH experiments in [8],[11]. The total noise in mesoscopic conductors at a finite temperature is called “quantum noise”. At finite temperatures, both temperature fluctuation and quantum fluctuation are significant. Thermal fluctuations are responsible for thermal noise, whereas quantum fluctuations are the origin of shot noise[10]. In this work, we have used a familiar setup in the context of chiral edge modes used in Ref. [12]. We extend these setups to both topological and trivial helical edge modes. We have shown distinct behaviour of chiral and helical edge modes and topological and trivial helical edge modes. The thermal noise-like contribution does not distinguish between chiral, topological, and trivial helical, but the shot noise-like contribution does in specific setups. The most striking result was that we could observe the different behaviour of trivial helical edge modes from topological helical edge modes by measuring both the quantum noise autocorrelation and cross-correlations.

This paper focuses on studying quantum noise in systems with different types of edge modes: chiral and helical (topological and trivial). In the next section, we

* colin.nano@gmail.com

explore the behaviour of quantum noise in the presence of chiral edge states by calculating cross-correlations between different terminals and autocorrelation in a four-terminal Hall bar. The terminals are connected to reservoirs with different chemical potentials. Section III extends our study to topological helical edge modes and calculates the quantum noise correlations. We also compare the results obtained for chiral and topological helical edge modes and find that they are distinct. In section IV, we study transport via trivial helical edge modes and find a distinct behaviour, as seen from the quantum noise correlations compared to topological helical edge modes. The results are justified by tables in the analysis section and an experimental realization in conclusion.

II. QUANTUM NOISE IN QUANTUM HALL SETUP

A. Theory

The current-current correlation between metallic contacts α and β is given by [10],

$$S_{\alpha\beta}(t-t') = \frac{1}{2} \langle \Delta \hat{I}_\alpha(t) \Delta \hat{I}_\beta(t') + \Delta \hat{I}_\beta(t') \Delta \hat{I}_\alpha(t) \rangle, \quad (1)$$

where $\Delta \hat{I}_\alpha(t)$ is the fluctuation in current from the average value in contact α and is given by $\Delta \hat{I}_\alpha(t) = \hat{I}_\alpha - \langle \hat{I}_\alpha \rangle$. For a multiterminal system, the current in contact α is given by [10],

$$\hat{I}_\alpha(t) = \frac{e}{2\pi\hbar} \sum_{\beta\gamma} \sum_{mn} \int dE dE' e^{i(E-E')t/\hbar} \hat{a}_{\beta m}^\dagger(E) A_{\beta\gamma}^{mn}(\alpha; E, E') \hat{a}_{\gamma n}(E'), \quad (2)$$

where summation over β, γ runs over the contacts except α , summation over m, n runs over number of edge channels. $\hat{a}_{\beta m}^\dagger(E)$ is the creation operator, which creates a particle (Boson or Fermion) with energy E in the terminal β in the edge channel m . Similarly, $\hat{a}_{\gamma n}(E')$ is the annihilation operator which annihilates a particle (Boson or Fermion) with energy E' in terminal γ in the edge channel n . Using these two operators, we can find the occupation number of the incident charge carriers in the terminal β in the edge channel m , given by,

$$\hat{n}_{\beta m}(E) = \hat{a}_{\beta m}^\dagger(E) \hat{a}_{\beta m}(E), \quad (3)$$

In eq. (2), $A_{\beta\gamma}^{mn}(\alpha; E, E')$ is given by [10],

$$A_{\beta\gamma}^{mn}(\alpha; E, E') = \delta_{mn} \delta_{\alpha\beta} \delta_{\alpha\gamma} - \sum_k s_{\alpha\beta;mk}^\dagger(E) s_{\alpha\gamma;kn}(E'). \quad (4)$$

where $s_{\alpha\beta;mk}(E)$ is the amplitude for an electron to scatter from terminal β in the edge channel k to terminal α in the edge channel m with energy E . Similarly, average

current in terminal α is given by,

$$\langle I_\alpha \rangle = \frac{e^2}{2\pi\hbar} \sum_\beta V_\beta \int dE \left(-\frac{\partial f}{\partial E} \right) \left[N_\alpha \delta_{\alpha\beta} - \text{Tr}(s_{\alpha\beta}^\dagger s_{\alpha\beta}) \right]. \quad (5)$$

where V_β is the applied voltage to contact β with $\beta \neq \alpha$. We can calculate the current fluctuation using Eq. (2) and Eq. (5) and derive the noise. The Fourier transform of Eq. (1) is called quantum noise, which is given by,

$$2\pi\delta(\omega + \omega') S_{\alpha\beta}^q(\omega) = \frac{1}{2} \langle \Delta \hat{I}_\alpha(\omega) \Delta \hat{I}_\beta(\omega') + \Delta \hat{I}_\beta(\omega') \Delta \hat{I}_\alpha(\omega) \rangle. \quad (6)$$

We can derive an expression for quantum noise [10] using Eqs. (2), (5) and (6) and the Fermi-Dirac statistics, we get,

$$S_{\alpha\beta}^q(\omega) = \frac{e^2}{2\pi\hbar} \sum_{\gamma,\delta} \sum_{mn} \int dE \text{Tr}[A_{\gamma\delta}^{mn}(\alpha; E, E + \hbar\omega) A_{\delta\gamma}^{mn}(\beta; E + \hbar\omega, E) (f_\gamma(E)[1 - f_\delta(E + \hbar\omega)] + [1 - f_\gamma(E)]f_\delta(E + \hbar\omega))]. \quad (7)$$

Our focus will be on zero frequency quantum noise, and for simplicity, we consider single edge mode occupation, which reduces Eq. (7) to,

$$S_{\alpha\beta}^q = \frac{e^2}{2\pi\hbar} \sum_{\gamma,\delta} \int dE \text{Tr}[A_{\gamma\delta}(\alpha) A_{\delta\gamma}(\beta) (f_\gamma(E)[1 - f_\delta(E)] + [1 - f_\gamma(E)]f_\delta(E))]. \quad (8)$$

where, $A_{\beta\gamma}(\alpha) = I_\alpha \delta_{\alpha\beta} \delta_{\alpha\gamma} - s_{\alpha\beta}^\dagger s_{\alpha\gamma}$, and $s_{\alpha\beta}$ is an element of the s-matrix of the setup, describing the amplitude for an electron to scatter from terminal β to α . $s_{\alpha\beta}$ is the scattering amplitude for an electron to scatter from terminal β to terminal α . f_γ is the Fermi Dirac distribution function for contact γ i.e., $f_\gamma = (1 + e^{(E - \mu_\gamma)/k_B T})^{-1}$, T is temperature of the system, μ_γ is the chemical potential of contact γ . Quantum noise, as in Eq. (8), contains two parts: (i) the thermal noise-like contribution and (ii) the shot noise-like contribution. The expression for both thermal and shot noise can be derived separately, and the full calculation is given in Appendix B. The thermal noise-like contribution comes due to the equilibrium current fluctuation. The shot noise contribution can be calculated by subtracting the thermal-like noise from the total quantum noise. Thus, $S_{\alpha\beta}^q = S_{\alpha\beta}^{th} + S_{\alpha\beta}^{sh}$, and

$$S_{\alpha\beta}^{th} = -\frac{2e^2}{h} \int dE [T_{\alpha\beta} f_\beta (1 - f_\beta) + T_{\beta\alpha} f_\alpha (1 - f_\alpha)],$$

$$S_{\alpha\beta}^{sh} = -\frac{2e^2}{h} \int \sum_{\gamma,\delta} (f_\gamma - f_\alpha) (f_\delta - f_\beta) \text{Tr}(s_{\alpha\gamma}^\dagger s_{\alpha\delta} s_{\beta\delta}^\dagger s_{\beta\gamma}). \quad (9)$$

f_γ, f_δ are the Fermi-Dirac distributions with chemical potentials μ_γ and μ_δ . Here $s_{\alpha\beta}$ is the scattering amplitude

for an electron to scatter from terminal β to terminal α . For our purpose, f_a and f_b are energy-dependent functions, which are Fermi-Dirac distributions. $T_{\alpha\beta}$ is the transmission probability for an electron to scatter from terminal β to terminal α .

Similarly, we can derive the thermal and shot noise-like contributions separately from the autocorrelation ($\alpha = \beta$). The thermal noise-like contribution to the autocorrelation is given as

$$S_{\alpha\alpha}^{th} = \frac{4e^2}{h} \int dE f_{\alpha}(1 - f_{\alpha}) \sum_{\beta \neq \alpha} T_{\alpha\beta}, \quad (10)$$

Similarly, the shot noise-like contribution is

$$S_{\alpha\alpha}^{sh} = \frac{2e^2}{h} \int dE \left(\sum_{\gamma} T_{\alpha\gamma} (f_{\gamma} - f_{\alpha}) + M_{\alpha} f_{\alpha}^2 - \sum_{\gamma, \delta} f_{\gamma} f_{\delta} Tr(s_{\alpha\gamma}^{\dagger} s_{\alpha\delta} s_{\alpha\delta}^{\dagger} s_{\alpha\gamma}) \right). \quad (11)$$

Here M_{α} is the number of edge modes in terminal α .

We consider a 4-terminal system with QH edge modes. We can apply voltages at any of the contacts and measure the current-current correlation between any contacts based on a system as in Fig. (1). We have three setups: setup 1 with $\mu_2 = \mu_3 = \mu_0$ and $\mu_1 = \mu_4 = \mu$, setup 2 with $\mu_2 = \mu_4 = \mu_0$ and $\mu_1 = \mu_3 = \mu$, setup 3 with $\mu_3 = \mu_4 = \mu_0$ and $\mu_1 = \mu_2 = \mu$. In each setup, we have a constriction with scattering amplitudes r, t respectively, and the general s-matrix for this quantum Hall bar, which is valid for each of the three setups, is given as,

$$s = \begin{pmatrix} 0 & te^{i\theta} & 0 & -ire^{i\theta} \\ 0 & 0 & e^{i\phi_2} & 0 \\ 0 & -ire^{i\theta} & 0 & te^{i\theta} \\ e^{i\phi_1} & 0 & 0 & 0 \end{pmatrix}. \quad (12)$$

The phases ϕ_2 and ϕ_1 are the propagating phases connecting different contacts due to the path difference of the electron. θ is the phase acquired when there is scattering due to the constriction. There will be an extra phase $\pi/2$ whenever there is a reflection due to the constriction to make the s-matrix unitary. We herein analyze the thermal and shot noise-like contributions and the quantum noise calculation for each setup.

B. Quantum noise due to chiral edge modes

1. Setup 1 [$\mu_2 = \mu_3 = \mu_0$ and $\mu_1 = \mu_4 = \mu$]

FIG. 1 shows a quantum Hall setup, which is characterized by $\mu_2 = \mu_3 = \mu_0$ and $\mu_1 = \mu_4 = \mu = \mu_0 + eV$, where V is the applied voltage. In this setup, all contacts are assumed to be ideal. In this case, we will analyze all current correlations between different contacts. For the quantum noise correlation between terminals: 1 and 3,

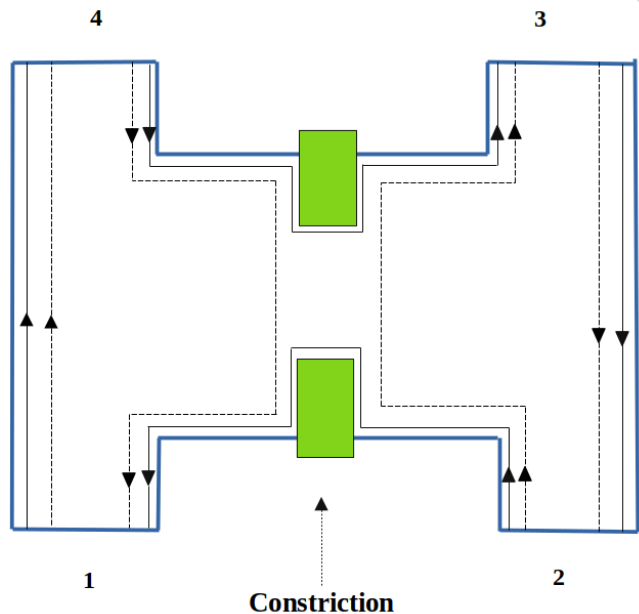


FIG. 1: Four terminal Quantum Hall Sample has chiral edge modes with a constriction. The black solid (dashed)line depicts the edge mode for a spin-up (spin-down) electron, which can transmit(reflect) via constriction

i.e., S_{13}^q , the thermal noise vanishes, and only shot noise contributes. We can see this below,

$$S_{13}^{sh} = -\frac{2e^2}{h} \int \sum_{\gamma, \delta=1,4} (f_{\gamma} - f_a)(f_{\delta} - f_b) Tr(s_{1\gamma}^{\dagger} s_{1\delta} s_{3\delta}^{\dagger} s_{3\gamma}), \quad (13)$$

f and f_0 are the Fermi-Dirac distribution function for terminals 1, 4 and 2, 3 according to the assumption as mentioned earlier. f_a and f_b are any energy-dependent function, which significance is explained in Appendix C. Choosing f_a and f_b to be f_0 , which is similar to the assumption taken in [12] and using the s-matrix given in Eq. (12), we get

$$S_{13}^q = S_{13}^{sh} = -\frac{2e^2}{h} \int dE RT (f - f_0)^2, \quad (14)$$

where $T = |s_{12}|^2 = |s_{14}|^2$ is the transmission probability of the constriction. The integration [13] in Eq. (14) is

$$\int_0^{\infty} dE (f - f_0)^2 = (\mu - \mu_0) \coth \left[\frac{(\mu - \mu_0)}{2k_B \mathcal{T}} \right] - 2k_B \mathcal{T}, \quad (15)$$

we have assumed the condition $\mu, \mu_0 \gg k_B \mathcal{T}$ and taken the lower limit to be 0 as we assume it to be the energy at the bottom of the conduction band. So, the quantum noise correlation between the terminals 1 and 3 is,

$$S_{13}^q = -\frac{2e^2}{h} RT \left[(\mu - \mu_0) \coth \left[\frac{(\mu - \mu_0)}{2k_B \mathcal{T}} \right] - 2k_B \mathcal{T} \right]. \quad (16)$$

The thermal noise-like contribution vanishes since the probability of the electron scattering from terminal 1 to 3, and vice versa is zero. Thus,

$$S_{13}^{th} = 0. \quad (17)$$

The quantum noise correlation between contacts 1 and 4 is denoted by S_{14}^q . The thermal noise like contribution to the quantum noise correlation S_{14}^{th} is given by,

$$S_{14}^{th} = -\frac{2e^2}{h} \int dE [T_{14} f_4 (1 - f_4) + T_{41} f_1 (1 - f_1)], \quad (18)$$

now, using $\int_0^\infty dE f_\alpha (1 - f_\alpha) = k_B \mathcal{T}$, where $\alpha = 1, 2, 3, 4$ with \mathcal{T} being the temperature, we get,

$$S_{14}^{th} = -\frac{2e^2}{h} k_B \mathcal{T} (T_{14} + T_{41}) = -\frac{2e^2}{h} k_B \mathcal{T} (1 + R), \quad (19)$$

wherein R is the reflection probability of the constriction. The above equation is the thermal noise-like contribution. Similarly, we can calculate the shot noise-like contribution, which is given as

$$S_{14}^{sh} = -\frac{2e^2}{h} \int \sum_{\gamma, \delta=1,4} (f_\gamma - f_a)(f_\delta - f_b) Tr(s_{1\gamma}^\dagger s_{1\delta} s_{4\delta}^\dagger s_{4\gamma}). \quad (20)$$

we see the shot noise contribution S_{14}^{sh} vanishes. So, the quantum noise correlation between probes 1 and 4 is entirely due to thermal noise. Thus,

$$S_{14}^q = S_{14}^{th} = -\frac{2e^2}{h} k_B \mathcal{T} (1 + R). \quad (21)$$

Similarly, when we calculate the quantum noise correlation between contacts 1 and 2, 3 and 4, and 2 and 3, we see that only thermal noise contributes, i.e.,

$$S_{12}^q = S_{34}^q = \frac{1 - R}{1 + R} S_{14}^q, \quad S_{23}^q = S_{14}^q. \quad (22)$$

There is one particular case as well, i.e., the quantum noise correlation between terminals 2 and 4 is precisely zero since both the thermal noise and shot noise-like contributions vanish. Similarly, we can calculate autocorrelation for each of the terminals. For this purpose, we have to use the formula for finite temperature quantum noise given in Eq. (1), the case $\alpha = \beta$. The autocorrelation in contact 1 is,

$$S_{11}^q = \frac{e^2}{2\pi\hbar} \sum_{\gamma, \delta=1,4} \int dE Tr[A_{\gamma\delta}(1) \quad (23)$$

$$A_{\delta\gamma}(1)] \times (f_\gamma(E)[1 - f_\delta(E)] + [1 - f_\gamma(E)]f_\delta(E)),$$

Using the s -matrix, we get the above quantity to be

$$S_{11}^q = \frac{2e^2}{h} \int [f(1 - f) + Rf(1 - f) + Tf_0(1 - f_0) + RT(f - f_0)^2]. \quad (24)$$

Similarly, the autocorrelation in contact 3: S_{33}^q is the same as S_{11}^q . Doing the integration in Eq. (24),

$$S_{11}^q = S_{33}^q = \frac{2e^2}{h} k_B \mathcal{T} [1 + R + T - 2RT] + \frac{2e^2}{h} RT \left[(\mu - \mu_0) \coth \left[\frac{(\mu - \mu_0)}{2k_B \mathcal{T}} \right] \right]. \quad (25)$$

Eq. (25) has both the thermal noise contribution and the shot noise-like contribution. Similarly, we can calculate auto-correlation in other terminals as well. The auto-correlation in other terminals is as follows:

$$S_{22}^q = S_{44}^q = \frac{4e^2}{h} k_B \mathcal{T}. \quad (26)$$

The autocorrelation in terminals 2 and 4 are the same, and they are thermal noise only.

2. setup 2 [$\mu_2 = \mu_4 = \mu_0$ and $\mu_1 = \mu_3 = \mu$]

In this subsection, we are concerned with the outcomes for setup 2, i.e., $\mu_2 = \mu_4 = \mu_0$ and $\mu_1 = \mu_3 = \mu = \mu_0 + eV$, where V is the applied voltage. Using the formulae given in Eq. (9), we can find the thermal and shot noise-like contributions to total quantum noise. The thermal noise-like contribution to the cross-correlation between the terminals will remain unchanged in any setup since it only depends on the transmission probability for the electron to scatter from one terminal to another and not on how voltage biases are applied. The shot noise-like contribution may change depending on voltage bias across the terminals. Below we provide a list of cross-correlations, which are only thermal noise-like.

$$S_{14}^q = S_{14}^{th} = S_{23}^q = S_{23}^{th} = -\frac{2e^2}{h} k_B \mathcal{T} (1 + R), \quad (27)$$

$$\text{and, } S_{12}^q = S_{12}^{th} = S_{34}^q = S_{34}^{th} = \frac{1 - R}{1 + R} S_{14}^q. \quad (28)$$

In all these cases, the shot noise-like contribution vanishes.

Further, the shot noise-like contribution to the quantum noise correlation between terminals 1 and 3 becomes zero, which was non-zero for setup 1. The shot noise-like contribution to the cross-correlation between terminals 2 and 4 is non-zero, which was zero for setup 1. The quantum noise correlation between terminals 1 and 3, 2 and 4 are given for setup 2, as below,

$$S_{13}^q = S_{13}^{sh} = S_{13}^{th} = 0, \quad (29)$$

$$S_{24}^q = S_{24}^{sh} = -\frac{2e^2}{h} RT \left[(\mu - \mu_0) \coth \left[\frac{(\mu - \mu_0)}{2k_B \mathcal{T}} \right] - 2k_B \mathcal{T} \right]. \quad (30)$$

The thermal noise-like contribution S_{24}^{th} is zero since the transmission probability T_{24} is zero. The autocorrelations in each terminal are the same, which is only thermal

noise-like and is

$$\begin{aligned} S_{11}^q = S_{11}^{th} = S_{22}^q = S_{22}^{th} = S_{33}^q = S_{33}^{th} = S_{44}^q = S_{44}^{th} \\ = \frac{2e^2}{h} 2k_B \mathcal{T}. \end{aligned} \quad (31)$$

3. *setup 3* [$\mu_1 = \mu_2 = \mu$ and $\mu_3 = \mu_4 = \mu_0$]

In this setup, we see that the quantum noise correlation between terminals 1 and 3, 2 and 4 are both shot noise-like only. The quantum noise-like correlation for other terminals is thermal noise-like. Below, we provide expressions of all the possible quantum noise cross-correlations.

$$\begin{aligned} S_{14}^q = S_{14}^{th} = S_{23}^q = S_{23}^{th} = -\frac{2e^2}{h} k_B \mathcal{T} (1 + R), \\ S_{12}^q = S_{12}^{th} = S_{34}^q = S_{34}^{th} = -\frac{(1-R)}{1+R} S_{14}^q, \\ S_{13}^q = S_{13}^{sh} = S_{24}^q = S_{24}^{sh} = -\frac{2e^2}{h} RT \\ \left[(\mu - \mu_0) \coth \left[\frac{(\mu - \mu_0)}{2k_B \mathcal{T}} \right] - 2k_B \mathcal{T} \right]. \end{aligned} \quad (32)$$

For the autocorrelations, we get,

$$\begin{aligned} S_{22}^q = S_{22}^{th} = S_{44}^q = S_{44}^{th} = \frac{4e^2}{h} k_B \mathcal{T}, \\ S_{33}^q = S_{11}^q = S_{22}^q + S_{11}^{sh}. \end{aligned} \quad (33)$$

where, $S_{11}^{sh} = S_{33}^{sh} = \frac{2e^2}{h} RT \left[(\mu - \mu_0) \coth \left[\frac{\mu - \mu_0}{2k_B \mathcal{T}} \right] - 2k_B \mathcal{T} \right]$. We observe that the quantum noise cross and autocorrelations are constant in some cases, whereas it changes symmetrically with the applied voltage ($eV = \mu - \mu_0$) in each setup. In the following section, we will calculate the quantum noise correlations in the presence of helical edge modes.

III. QUANTUM NOISE IN QUANTUM SPIN HALL SETUP

A. Theory

The current-current correlation between the metallic contacts α and β due to spin polarised current is given by,

$$S_{\alpha\beta}^{\sigma\sigma'}(t-t') = \frac{1}{2} \langle \Delta \hat{I}_\alpha^\sigma(t) \Delta \hat{I}_\beta^{\sigma'}(t') + \Delta \hat{I}_\beta^{\sigma'}(t') \Delta \hat{I}_\alpha^\sigma(t) \rangle, \quad (34)$$

where $\Delta \hat{I}_\alpha^\sigma$ is the fluctuation in current from the average value in contact α with spin σ and is given by $\Delta \hat{I}_\alpha^\sigma = \hat{I}_\alpha^\sigma - \langle \hat{I}_\alpha^\sigma \rangle$. The current due to a charged particle with

spin σ flowing through terminal α is

$$\begin{aligned} \hat{I}_\alpha^\sigma(t) = \frac{e}{h} \sum_{n=1}^M \int \int dE dE' e^{i(E-E')t/\hbar} \\ \times (\hat{a}_{\alpha n}^{\sigma\dagger}(E) \hat{a}_{\alpha n}^\sigma(E') - \hat{b}_{\alpha n}^{\sigma\dagger}(E) \hat{b}_{\alpha n}^\sigma(E')), \end{aligned} \quad (35)$$

where $\hat{a}_{\alpha n}^{\sigma\dagger}(E)$ is the creation operator, which creates an incoming electron in terminal α with energy E in edge channel n and $\hat{a}_{\alpha n}^\sigma(E)$ is the annihilation operator, which annihilates an incoming electron in the terminal α with energy E' in edge channel n . Similarly, $\hat{b}_{\alpha n}^{\sigma\dagger}(E)$ and $\hat{b}_{\alpha n}^\sigma(E')$ are the creation and annihilation operators, which create and annihilate an outgoing electron from the terminal α with spin σ with energy E and E' respectively. The expression for finite temperature quantum noise correlation in quantum spin Hall set up due to the spin polarised currents I^\uparrow and I^\downarrow see in Fig. 2 is given by,

$$S_{\alpha\beta}^q = S_{\alpha\beta}^{\uparrow\uparrow q} + S_{\alpha\beta}^{\uparrow\downarrow q} + S_{\alpha\beta}^{\downarrow\uparrow q} + S_{\alpha\beta}^{\downarrow\downarrow q}, \quad (36)$$

the individual spin polarised contributions are given as[14],

$$\begin{aligned} S_{\alpha\beta}^{\sigma\sigma'q} = \frac{e^2}{2\pi\hbar} \sum_{\rho,\rho'=\uparrow,\downarrow} \sum_{\gamma,\delta} \int dE T r [A_{\gamma\delta}^{\rho\rho'}(\alpha, \sigma) A_{\delta\gamma}^{\rho'\rho}(\beta, \sigma')] \\ (f_\gamma(E)[1 - f_\delta(E)] + [1 - f_\gamma(E)]f_\delta(E)), \end{aligned} \quad (37)$$

where, σ, σ' denotes the spin of electrons. Eq. (37) has both the thermal noise-like contribution and shot noise-like contribution to the quantum noise. We will first look into the cross-correlation, i.e., $\alpha \neq \beta$. The thermal noise-like contribution is given by;

$$S_{\alpha\beta}^{sth} = S_{\alpha\beta}^{\uparrow\uparrow th} + S_{\alpha\beta}^{\uparrow\downarrow th} + S_{\alpha\beta}^{\downarrow\uparrow th} + S_{\alpha\beta}^{\downarrow\downarrow th}, \quad (38)$$

and the individual spin polarised contributions to the thermal noise are given as,

$$S_{\alpha\beta}^{\sigma\sigma' th} = -\frac{2e^2}{h} \int_0^\infty dE [T_{\alpha\beta}^{\sigma\sigma'} f_\beta(1 - f_\beta) + T_{\beta\alpha}^{\sigma\sigma'} f_\alpha(1 - f_\alpha)]. \quad (39)$$

see Appendix C for the derivation of Eq. (39). $T_{\alpha\beta}^{\sigma\sigma'}$ is the transmission probability for an electron to scatter from terminal β with initial spin σ' to terminal α with final spin σ . f_β is the Fermi-Dirac distribution function at contact β connected to a reservoir given by the expression $f_\beta = (1 + e^{(E-\mu_\beta)/k_B \mathcal{T}})^{-1}$, where \mathcal{T} is the temperature of the system, μ_β is the chemical potential of the contact β .

Similar to Eq. (38), the shot noise-like contribution is

$$S_{\alpha\beta}^{sh} = S_{\alpha\beta}^{\uparrow\uparrow sh} + S_{\alpha\beta}^{\uparrow\downarrow sh} + S_{\alpha\beta}^{\downarrow\uparrow sh} + S_{\alpha\beta}^{\downarrow\downarrow sh}, \quad (40)$$

the individual spin-polarised contributions are

$$\begin{aligned} S_{\alpha\beta}^{\sigma\sigma' sh} = -\frac{2e^2}{h} \int dE \sum_{\gamma,\delta} \sum_{\rho\rho'=\uparrow,\downarrow} (f_\gamma - f_\alpha)(f_\delta - f_\beta) \\ \times T r (s_{\alpha\gamma}^{\sigma\rho\dagger} s_{\alpha\delta}^{\sigma\rho'} s_{\beta\delta}^{\sigma'\rho'\dagger} s_{\beta\gamma}^{\sigma'\rho}). \end{aligned} \quad (41)$$

See Appendix D for the derivation of Eq. (41).

Similarly, the quantum noise autocorrelation($\alpha = \beta$) is

$$S_{\alpha\alpha}^q = S_{\alpha\alpha}^{\uparrow\uparrow q} + S_{\alpha\alpha}^{\uparrow\downarrow q} + S_{\alpha\alpha}^{\downarrow\uparrow q} + S_{\alpha\alpha}^{\downarrow\downarrow q}, \quad (42)$$

where the individual spin-polarised correlations are

$$S_{\alpha\alpha}^{\sigma\sigma'q} = \frac{e^2}{2\pi\hbar} \sum_{\rho,\rho'=\uparrow,\downarrow} \sum_{\gamma,\delta} \int dE \text{Tr} [A_{\gamma\delta}^{\rho\rho'}(\alpha, \sigma) A_{\delta\gamma}^{\rho'\rho}(\alpha, \sigma')] \\ (f_{\gamma}(E)[1 - f_{\delta}(E)] + [1 - f_{\gamma}(E)]f_{\delta}(E)), \quad (43)$$

Eq. (43) also has both thermal noise-like and shot noise-like contributions. For the autocorrelation i.e. $\alpha = \beta$, the thermal noise like contribution is given by:

$$S_{\alpha\alpha}^{th} = S_{\alpha\alpha}^{\uparrow\uparrow th} + S_{\alpha\alpha}^{\uparrow\downarrow th} + S_{\alpha\alpha}^{\downarrow\uparrow th} + S_{\alpha\alpha}^{\downarrow\downarrow th}, \quad (44)$$

where the spin-polarised contributions, as derived in Appendix C, are given as

$$S_{\alpha\alpha}^{\sigma\sigma'th} = \frac{4e^2}{h} \int dE f_{\alpha}(1 - f_{\alpha}) \sum_{\alpha \neq \beta} T_{\alpha\beta}^{\sigma\sigma'}. \quad (45)$$

Similarly to thermal noise, shot noise contribution to the autocorrelation is,

$$S_{\alpha\alpha}^{sh} = S_{\alpha\alpha}^{\uparrow\uparrow sh} + S_{\alpha\alpha}^{\uparrow\downarrow sh} + S_{\alpha\alpha}^{\downarrow\uparrow sh} + S_{\alpha\alpha}^{\downarrow\downarrow sh}, \quad (46)$$

where, the spin polarised contribution, as derived in Appendix D, is given as,

$$S_{\alpha\alpha}^{\sigma\sigma'sh} = \frac{2e^2}{h} \int dE \left(\sum_{\gamma} T_{\alpha\gamma}^{\sigma\sigma'} (f_{\gamma} - f_{\alpha}) + \right. \\ \left. M_{\alpha} \delta_{\sigma\sigma'} f_{\alpha}^2 - \sum_{\gamma\delta} \sum_{\rho\rho'=\uparrow,\downarrow} \text{Tr} (s_{\alpha\gamma}^{\sigma\rho\dagger} s_{\alpha\delta}^{\rho'\rho'} s_{\alpha\delta}^{\sigma'\rho'\dagger} s_{\alpha\gamma}^{\sigma'\rho}) \right). \quad (47)$$

Here M_{α} is the number of edge modes from contact α .

B. Results for topological helical edge modes

This section considers a 4-terminal system with QSH edge modes, which is topological, and the electron motion is helical, as shown in FIG. 2. We can apply voltages at any contact and measure the current-current correlation between any of those contacts based on a system as in Fig. 2. In Fig. 2, we have a constriction with reflection and transmission amplitudes r , t , respectively. The general s -matrix for this quantum spin Hall bar setup is,

$$s = \begin{pmatrix} 0 & 0 & te^{i\theta} & 0 & 0 & 0 & -ire^{i\theta} & 0 \\ 0 & 0 & 0 & 0 & 0 & 0 & 0 & e^{i\phi_1} \\ 0 & 0 & 0 & 0 & e^{i\phi_2} & 0 & 0 & 0 \\ 0 & te^{i\theta} & 0 & 0 & 0 & -ire^{i\theta} & 0 & 0 \\ 0 & 0 & -ire^{i\theta} & 0 & 0 & 0 & te^{i\theta} & 0 \\ 0 & 0 & 0 & e^{i\phi_2} & 0 & 0 & 0 & 0 \\ e^{i\phi_1} & 0 & 0 & 0 & 0 & 0 & 0 & 0 \\ 0 & -ire^{i\theta} & 0 & 0 & 0 & te^{i\theta} & 0 & 0 \end{pmatrix} \quad (48)$$

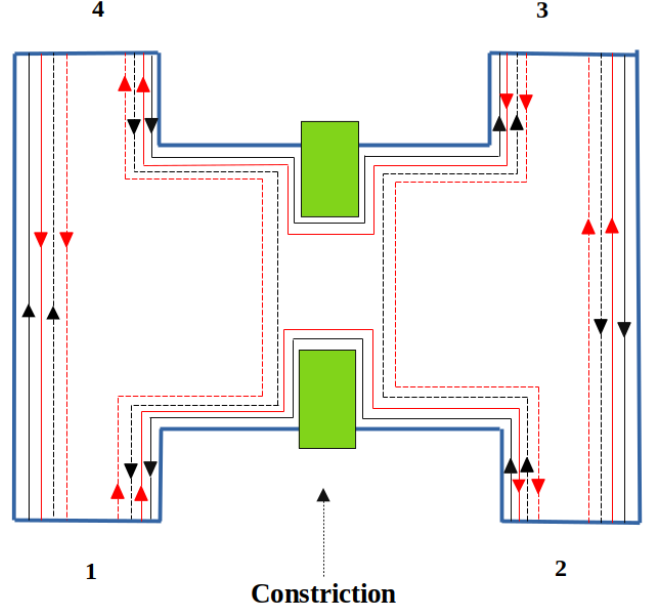


FIG. 2: Four terminal quantum Hall sample with a constriction, showing Helical edge modes. The Black(Red) solid (dashed)line depicts the edge mode for a spin-up (down) electron, which can transmit(reflect) via constriction.

The phases ϕ_1 and ϕ_2 are determined by the path difference for the electron reaching contacts 1, 2 from contacts 4, 3 or vice-versa, without scattering. θ is the phase acquired during transmission via the constriction. An extra phase $\pi/2$ occurs whenever there is scattering due to the constriction. The s -matrix is unitary as it is wont. We have three setups. Setup 1 is defined by parameters such that $\mu_2 = \mu_3 = \mu_0$ and $\mu_1 = \mu_4 = \mu$ condition holds. Similarly, Setup 2 is defined by $\mu_2 = \mu_4 = \mu_0$ and $\mu_1 = \mu_3 = \mu$ and setup 3 by $\mu_3 = \mu_4 = \mu_0$ and $\mu_1 = \mu_2 = \mu$. We herein analyze the thermal noise-like, shot noise, and quantum noise correlations in each setup using the s -matrix given in Eq. (48).

1. setup 1 [$\mu_1 = \mu_4 = \mu$ and $\mu_2 = \mu_3 = \mu_0$]

From the s matrix, we can calculate the thermal and shot noise-like contributions to the total quantum noise. We will examine the quantum noise cross correlation between the probes 1 and 4. The thermal noise-like contribution to the quantum noise is given by

$$S_{14}^{th} = S_{14}^{\uparrow\uparrow th} + S_{14}^{\uparrow\downarrow th} + S_{14}^{\downarrow\uparrow th} + S_{14}^{\downarrow\downarrow th}. \quad (49)$$

We first calculate $S_{14}^{\uparrow\uparrow th}$ as follows:

$$S_{14}^{\uparrow\uparrow th} = -\frac{2e^2}{h} \int dE [T_{14}^{\uparrow\uparrow} f_4(1 - f_4) + T_{41}^{\uparrow\uparrow} f_1(1 - f_1)]. \quad (50)$$

Making use of the integral $\int_0^\infty f_\alpha(1-f_\alpha) = k_B\mathcal{T}$ for $\mu, \mu_0 \gg k_B\mathcal{T}$, we get

$$S_{14}^{\uparrow\uparrow th} = -\frac{2e^2}{h}k_B\mathcal{T}[T_{14}^{\uparrow\uparrow} + T_{41}^{\uparrow\uparrow}] = -\frac{2e^2}{h}k_B\mathcal{T}(1+R). \quad (51)$$

Similar calculation shows, $S_{14}^{\downarrow\downarrow th} = 0$, $S_{14}^{\downarrow\uparrow th} = 0$, and $S_{14}^{\uparrow\downarrow th} = -\frac{2e^2}{h}k_B\mathcal{T}(1+R)$. Thus the thermal noise-like contribution to the quantum noise is given by $S_{14}^{th} = -\frac{4e^2}{h}k_B\mathcal{T}(1+R)$. R is the reflection probability for an electron to reflect from the constriction. Here, we can observe that the thermal noise-like contribution is twice that of the chiral quantum Hall case. The shot noise-like contribution to the quantum noise is given by,

$$S_{14}^{sh} = S_{14}^{\uparrow\uparrow sh} + S_{14}^{\downarrow\downarrow sh} + S_{14}^{\uparrow\downarrow sh} + S_{14}^{\downarrow\uparrow sh}, \quad (52)$$

The shot noise cross-correlation $S_{14}^{\sigma\sigma' sh}$ can be calculated from Eq. (47),

$$S_{14}^{\sigma\sigma' sh} = -\frac{2e^2}{h} \int dE \sum_{\gamma, \delta} \sum_{\rho\rho'=\uparrow, \downarrow} (f_\gamma - f_\alpha)(f_\delta - f_b) \times \text{Tr}(s_{1\gamma}^{\sigma\rho\dagger} s_{1\delta}^{\sigma\rho'} s_{4\delta}^{\sigma'\rho'\dagger} s_{4\gamma}^{\sigma\rho}). \quad (53)$$

Similar to chiral case, we consider $\mu_1 = \mu_4 = \mu = \mu_0 + eV$ and $\mu_2 = \mu_3 = \mu_0$. Once again, we consider the energy-dependent functions f_a and f_b equal to f_0 , which is the Fermi-Dirac distribution of contacts 2 and 3. Using the s -matrix, we get $S_{14}^{\uparrow\uparrow sh} = 0$. Similarly other correlations such as $S_{14}^{\uparrow\downarrow sh}$, $S_{14}^{\downarrow\uparrow sh}$ and $S_{14}^{\downarrow\downarrow sh}$ are also zero. Thus, the shot noise-like contribution to the quantum noise S_{14}^q vanishes. The quantum noise, however, is

$$S_{14}^q = S_{14}^{th} = -\frac{4e^2}{h}k_B\mathcal{T}(1+R). \quad (54)$$

Like the chiral case, the total contribution to the quantum noise comes from thermal noise only. Similarly, correlations between 1 and 2, 3 and 4, 2 and 3, and 1 and 4 show similar nature where only the thermal noise contributes to the quantum noise. These quantum noise correlations are given as

$$S_{12}^q = S_{34}^q = \frac{1-R}{1+R}S_{14}^q, \quad S_{23}^q = S_{14}^q. \quad (55)$$

We can see that the quantum noise correlation between terminals 2 and 4 is now finite, which was zero in the quantum Hall case. The noise correlation between these two terminals is pure shot noise-like. There is no thermal noise-like contribution.

$$S_{24}^q = S_{24}^{sh} = -\frac{4e^2}{h}RT \left[(\mu - \mu_0) \coth \left[\frac{(\mu - \mu_0)}{2k_B\mathcal{T}} \right] - 2k_B\mathcal{T} \right]. \quad (56)$$

It is a significant result since it distinguishes chiral edge modes from helical ones. As shown in Fig. 3, we have verified that for the chiral case, S_{24}^q is zero, but this is

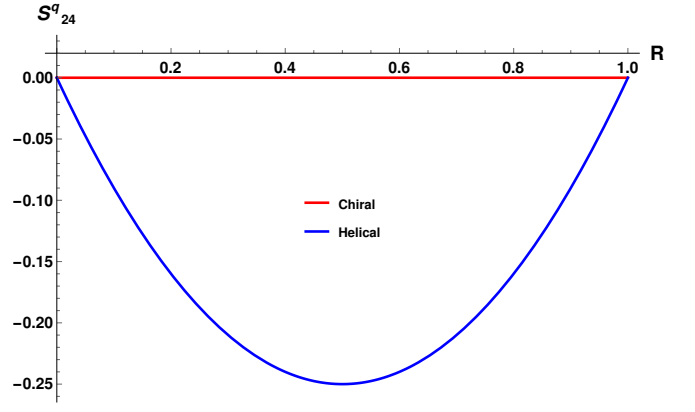


FIG. 3: Behaviour of quantum noise cross correlation between terminals 2 and 4 in units of $\frac{2e^2}{h}k_B\mathcal{T}$ with $(\mu - \mu_0 = 4)$ in units of $k_B\mathcal{T}$ in setup 1 for $\mu_1 = \mu_4 = \mu$ and $\mu_2 = \mu_3 = \mu_0$.

finite when the transport happens via helical edge modes. The quantum noise correlation between terminals 1 and 3 is only due to the shot noise-like contribution since the thermal noise-like contribution vanishes, which is the same for the chiral case, as shown in Fig. (16).

The quantum noise correlation between terminals 1 and 3 gives us,

$$S_{13}^q = S_{13}^{sh} = -\frac{4e^2}{h}RT \left[(\mu - \mu_0) \coth \left[\frac{(\mu - \mu_0)}{2k_B\mathcal{T}} \right] - 2k_B\mathcal{T} \right]. \quad (57)$$

Similarly, we calculate the autocorrelations as well. The autocorrelation in terminal 1 is,

$$S_{11}^q = S_{11}^{\uparrow\uparrow q} + S_{11}^{\downarrow\downarrow q} + S_{11}^{\uparrow\downarrow q} + S_{11}^{\downarrow\uparrow q}. \quad (58)$$

The thermal noise-like contribution to $S_{11}^{\uparrow\uparrow q}$ can be calculated from Eq. (45) and is given as,

$$S_{11}^{\uparrow\uparrow th} = \frac{4e^2}{h} \int_0^\infty dE f(1-f)(T_{12}^{\uparrow\uparrow} + T_{13}^{\uparrow\uparrow} + T_{14}^{\uparrow\uparrow}) = \frac{4e^2}{h}k_B\mathcal{T}. \quad (59)$$

where, $T_{12}^{\uparrow\uparrow} = T$, $T_{13}^{\uparrow\uparrow} = 0$ and $T_{14}^{\uparrow\uparrow} = R$.

Similarly, the shot noise-like contribution can be derived from Eq. (47) and is given by,

$$S_{11}^{\uparrow\uparrow sh} = \frac{2e^2}{h} \int dE \left(T_{12}^{\uparrow\uparrow} (f_0 - f) + f^2 - \sum_{\gamma\delta} \sum_{\rho\rho'=\uparrow, \downarrow} \text{Tr}(s_{1\gamma}^{\sigma\rho\dagger} s_{1\delta}^{\sigma\rho'} s_{1\delta}^{\sigma'\rho'\dagger} s_{1\gamma}^{\sigma\rho}) \right). \quad (60)$$

The quantum noise S_{11}^q is therefore,

$$S_{11}^{\uparrow\uparrow q} = \frac{2e^2}{h} \int [f(1-f) + Rf(1-f) + Tf_0(1-f_0) + RT(f-f_0)^2], \quad (61)$$

Which gives rise to,

$$S_{11}^{\uparrow\uparrow q} = \frac{2e^2}{h} k_B \mathcal{T} [1 + R + T - 2RT] + \frac{2e^2}{h} RT \left((\mu - \mu_0) \coth \left[\frac{(\mu - \mu_0)}{2k_B \mathcal{T}} \right] \right). \quad (62)$$

Similarly, other correlations can be calculated from Eq. (43), and they are,

$$S_{11}^{\uparrow\downarrow q} = S_{11}^{\downarrow\uparrow q} = 0, S_{11}^{\downarrow\downarrow q} = \frac{4e^2}{h} k_B \mathcal{T}, \quad (63)$$

Thus, the quantum noise autocorrelation in terminal 1 is,

$$S_{11}^q = \frac{2e^2}{h} k_B \mathcal{T} [3 + R + T - 2RT] + \frac{2e^2}{h} RT \left((\mu - \mu_0) \coth \left[\frac{(\mu - \mu_0)}{2k_B \mathcal{T}} \right] \right). \quad (64)$$

We can calculate the other autocorrelations as well, and we find all of them to be the same, i.e.,

$$S_{11}^q = S_{22}^q = S_{33}^q = S_{44}^q \quad (65)$$

However, we observe one profound difference. In the presence of chiral edge modes, the quantum noise S_{24}^q is pure thermal-like, but for helical edge modes, shot noise also contributes to autocorrelation. It distinguishes chiral from helical edge modes.

2. setup 2 [$\mu_1 = \mu_3 = \mu$ and $\mu_2 = \mu_4 = \mu_0$]

As explained earlier, the thermal noise-like contribution does not change for different cases. The quantum noise cross correlation between different terminals is,

$$S_{14}^q = S_{14}^{th} = S_{23}^q = S_{23}^{th} = -\frac{4e^2}{h} k_B \mathcal{T} (1 + R), \quad (66)$$

$$S_{12}^q = S_{34}^q = \frac{1 - R}{1 + R} S_{14}^q, \quad (67)$$

$$S_{13}^q = 0, \quad (68)$$

$$S_{24}^q = S_{24}^{sh} = -\frac{4e^2}{h} RT \left[(\mu - \mu_0) \coth \left[\frac{(\mu - \mu_0)}{2k_B \mathcal{T}} \right] - 2k_B \mathcal{T} \right]. \quad (69)$$

Above Eqs. imply $S_{14}^{sh} = S_{23}^{sh} = S_{12}^{sh} = S_{34}^{sh} = 0$ and $S_{24}^{th} = 0$. In this setup, we do not have any examples showing distinct results for chiral and helical edge modes. The autocorrelation for quantum noise in this setup is only thermal noise, i.e.,

$$S_{11}^q = S_{11}^{th} = S_{22}^q = S_{22}^{th} = S_{33}^q = S_{33}^{th} = S_{44}^q = S_{44}^{th} = \frac{2e^2}{h} 4k_B \mathcal{T}. \quad (70)$$

Here the shot noise contributions to each quantum noise correlation vanish, i.e., $S_{11}^{sh} = S_{22}^{sh} = S_{33}^{sh} = S_{44}^{sh} = 0$.

3. setup 3 [$\mu_1 = \mu_2 = \mu$ and $\mu_3 = \mu_4 = \mu_0$]

For this setup, the thermal noise-like contribution does not change, but the shot noise-like contribution to the quantum noise cross-correlation S_{13}^q , S_{24}^q are non-zero now. We do not see different results for chiral and helical edge modes in this setup. The quantum noise cross-correlation between different terminals is

$$\begin{aligned} S_{14}^q &= S_{14}^{th} = S_{23}^q = S_{23}^{th} = -\frac{4e^2}{h} k_B \mathcal{T} (1 + R), \\ S_{12}^q &= S_{12}^{th} = S_{34}^q = S_{34}^{th} = \frac{1 - R}{1 + R} S_{14}^q, \\ S_{13}^q &= S_{13}^{sh} = S_{24}^q = S_{24}^{th} = -\frac{4e^2}{h} RT \left[(\mu - \mu_0) \coth \left[\frac{(\mu - \mu_0)}{2k_B \mathcal{T}} \right] - 2k_B \mathcal{T} \right]. \end{aligned} \quad (71)$$

Here, Eq. (71) implies that

$$\begin{aligned} S_{14}^{sh} &= S_{23}^{sh} = S_{12}^{sh} = S_{34}^{sh} = 0, \\ S_{13}^{th} &= S_{24}^{th} = 0. \end{aligned} \quad (72)$$

Similarly, the quantum noise autocorrelations are

$$\begin{aligned} S_{11}^q &= S_{22}^q = \frac{2e^2}{h} \int dE (4f(1-f) + 2RT(f-f_0)^2), \\ S_{33}^q &= S_{44}^q = \frac{2e^2}{h} \int dE (4f_0(1-f_0) + 2RT(f-f_0)^2). \end{aligned} \quad (73)$$

which, on integrating, give

$$\begin{aligned} S_{11}^q &= S_{22}^q = S_{33}^q = S_{44}^q = \frac{2e^2}{h} 4k_B \mathcal{T} + \\ &\frac{2e^2}{h} RT \left[(\mu - \mu_0) \coth \left[\frac{(\mu - \mu_0)}{2k_B \mathcal{T}} \right] - 2k_B \mathcal{T} \right]. \end{aligned} \quad (74)$$

Here thermal noise-like contributions are given as,

$$S_{11}^{th} = S_{22}^{th} = S_{33}^{th} = S_{44}^{th} = \frac{2e^2}{h} 4k_B \mathcal{T}, \quad (75)$$

and the shot noise-like contributions are given as,

$$\begin{aligned} S_{11}^{sh} &= S_{22}^{sh} = S_{33}^{sh} = S_{44}^{sh} \\ &= \frac{2e^2}{h} RT \left[(\mu - \mu_0) \coth \left[\frac{(\mu - \mu_0)}{2k_B \mathcal{T}} \right] - 2k_B \mathcal{T} \right]. \end{aligned} \quad (76)$$

In this setup, we also see a difference, i.e., the autocorrelations S_{22}^q and S_{44}^q are thermal noise-like for chiral edge modes and for the transport via helical edge modes, they are the sum of thermal and shot noise-like contributions.

Due to the existence of helical edge modes, the shot noise contributes in some cases, such as S_{24}^q in setup 1, and S_{22}^q , S_{44}^q in setups 1 and 3, which makes the total quantum noise results for the helical case distinct from the chiral case, as has been highlighted in Fig. 4(a).

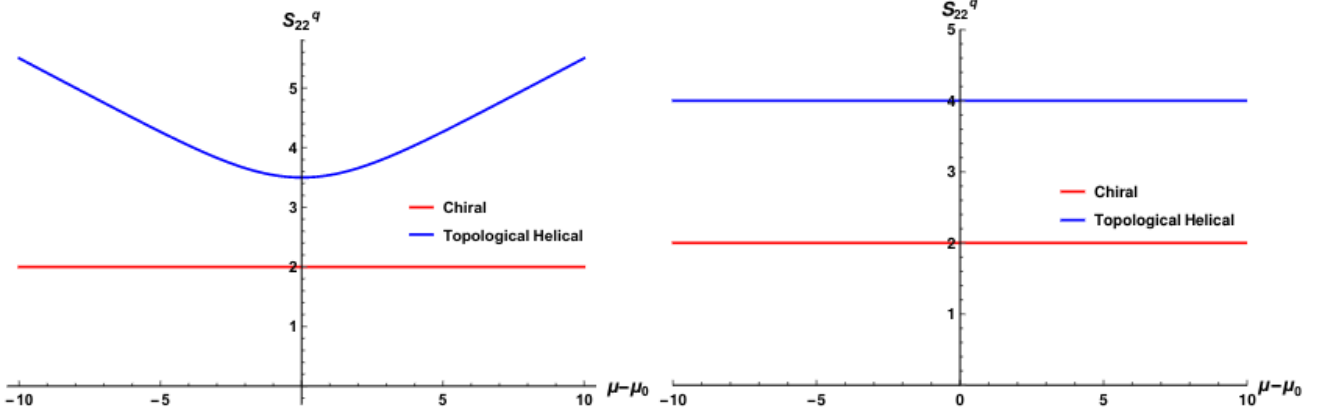


FIG. 4: (a) Quantum noise autocorrelation $S_{22}^q = S_{44}^q$ in setup 1 (Results are identical in setup 3 as well) and (b) Quantum noise autocorrelation $S_{11}^q = S_{22}^q = S_{33}^q = S_{44}^q$ in Setup 2 in units of $\frac{2e^2}{h}k_B\mathcal{T}$ versus the voltage bias $(\mu - \mu_0)$ in units of $k_B\mathcal{T}$ with $R = 0.5$ and $\mu_0 = 100k_B\mathcal{T}$.

C. Results for trivial Helical edge modes

We consider a trivial quantum spin Hall setup shown in Fig. 5. In this case, up spin electron can get backscattered as a spin-down electron preserving spin-momentum locking[8]. In this situation, the electron has a finite probability p for a change in its direction of motion and spin with the help of intraedge scattering. In Ref. [11], the topological and trivial helical edge modes are differentiated via non-local resistance measurements by tuning electric and magnetic fields. In our work, we will show how the topological and trivial helical edge modes two

different helical edge modes are distinguished from each other via quantum noise cross-correlations as well as autocorrelations.

Similar to chiral and topological helical setups, we can apply different voltages at any of the contacts and measure quantum noise cross and autocorrelation in the trivial QSH setup. Here, we work with three different setups similar to that used for transport via topological helical edge modes. Here, in addition to scattering from the constriction, we have spin-flip scattering, and the general s -matrix for this system, as shown in Fig. 5, is

$$s = \begin{pmatrix} 0 & -i\sqrt{p} & te^{i\theta}\sqrt{1-p} & 0 & 0 & 0 & -ire^{i\theta}\sqrt{1-p} & 0 \\ -i\sqrt{p} & 0 & 0 & 0 & 0 & 0 & 0 & \sqrt{(1-p)}e^{i\phi_1} \\ 0 & 0 & 0 & -i\sqrt{p} & \sqrt{(1-p)}e^{i\phi_2} & 0 & 0 & 0 \\ 0 & te^{i\theta}\sqrt{1-p} & -i\sqrt{p} & 0 & 0 & -ire^{i\theta}\sqrt{1-p} & 0 & 0 \\ 0 & 0 & -ire^{i\theta}\sqrt{1-p} & 0 & 0 & -i\sqrt{p} & te^{i\theta}\sqrt{1-p} & 0 \\ 0 & 0 & 0 & \sqrt{(1-p)}e^{i\phi_2} & -i\sqrt{p} & 0 & 0 & 0 \\ \sqrt{(1-p)}e^{i\phi_1} & 0 & 0 & 0 & 0 & 0 & 0 & -i\sqrt{p} \\ 0 & -ire^{i\theta}\sqrt{1-p} & 0 & 0 & 0 & te^{i\theta}\sqrt{1-p} & -i\sqrt{p} & 0 \end{pmatrix}, \quad (77)$$

At $p = 0$, we correctly reproduce the s -matrix for topological helical edge modes. We herein analyze the thermal noise, shot noise, and quantum noises using the s matrix given in Eq. (74).

1. setup 1 [$\mu_1 = \mu_4 = \mu$ and $\mu_2 = \mu_3 = \mu_0$]

From Eq. (74), we can find thermal and shot noise, like contribution to quantum noise cross and autocorrelations. For this setup, the thermal noise-like contribution

to quantum noise correlation between terminals 1 and 4 is,

$$S_{14}^{th} = S_{14}^{\uparrow\uparrow th} + S_{14}^{\uparrow\downarrow th} + S_{14}^{\downarrow\uparrow th} + S_{14}^{\downarrow\downarrow th}. \quad (78)$$

The quantity $S_{14}^{\uparrow\uparrow th}$ can be found from Eq. (39),

$$S_{14}^{\uparrow\uparrow th} = -\frac{2e^2}{h} \int dE [T_{14}^{\uparrow\uparrow} f_4(1-f_4) + T_{41}^{\uparrow\uparrow} f_1(1-f_1)], \quad (79)$$

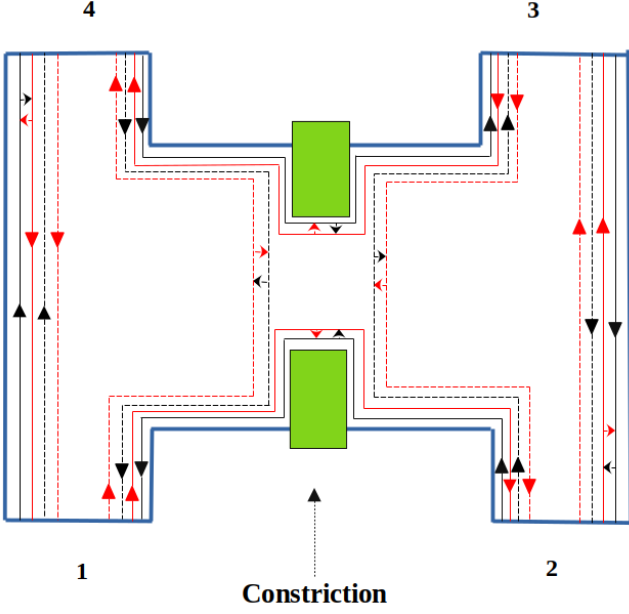


FIG. 5: Four terminal Quantum Spin Hall Sample having trivial edge modes with a constriction. The black solid and dashed line depicts the edge mode for a spin-up electron, and the red solid and dashed line depicts the edge mode for a spin-down electron. Solid lines are for the edge modes transmitting, and dashed lines are for the edge modes reflecting via constriction.

Again, making use of integration $\int_0^\infty dE f_\alpha (1 - f_\alpha) = k_B \mathcal{T}$ for $\alpha = 1, 2, 3, 4$, for $\mu, \mu_0 \gg k_B \mathcal{T}$.

$$S_{14}^{\uparrow th} = -\frac{2e^2}{h} k_B \mathcal{T} (1 + R) (1 - p). \quad (80)$$

Similarly, we can calculate other spin polarised components such as $S_{14}^{\uparrow \downarrow th}$, $S_{14}^{\downarrow \uparrow th}$ and $S_{14}^{\downarrow \downarrow th}$. The thermal noise like contribution S_{14}^{th} is given by

$$S_{14}^{th} = -\frac{4e^2}{h} k_B \mathcal{T} (1 + R) (1 - p). \quad (81)$$

Now, for the calculation of shot noise like contribution to the quantum noise, we will use Eq. (41). The spin polarised contribution shot noise like contribution to the quantum noise S_{14}^q is

$$S_{14}^{\sigma\sigma' sh} = -\frac{2e^2}{h} \int dE \sum_{\gamma, \delta=1,4} \sum_{\rho\rho'=\uparrow, \downarrow} (f_\gamma - f_0)(f_\delta - f_0) \text{Tr}(s_{1\gamma}^{\sigma\rho\dagger} s_{1\delta}^{\sigma\rho'} s_{4\delta}^{\sigma'\rho'\dagger} s_{4\gamma}^{\sigma'\rho}). \quad (82)$$

We have also considered the energy-dependent functions f_a and f_b to be f_0 since the assumption taken in Eq.(6) is still valid here.

After calculating the above correlation, we get,

$$S_{14}^{\uparrow sh} = S_{14}^{\downarrow sh} = 0, \quad (83)$$

$$S_{14}^{\downarrow \uparrow sh} = -\frac{2e^2}{h} 4p(1-p) \int dE (f - f_0)^2, \quad (84)$$

$$S_{14}^{\uparrow \downarrow sh} = (1 - T) S_{14}^{\downarrow \uparrow sh}. \quad (85)$$

Using $\int_0^\infty (f - f_0)^2 = (\mu - \mu_0) \coth \left[\frac{(\mu - \mu_0)}{2k_B \mathcal{T}} \right] - 2k_B \mathcal{T}$, we get the total quantum noise correlation between terminals 1 and 4, $S_{14}^q = S_{14}^{th} + S_{14}^{sh}$ to be,

$$S_{14}^q = -\frac{2e^2}{h} (1 - p) (1 + R) \left(2k_B \mathcal{T} + 4p \left[(\mu - \mu_0) \coth \left[\frac{\mu - \mu_0}{2k_B \mathcal{T}} \right] - 2k_B \mathcal{T} \right] \right). \quad (86)$$

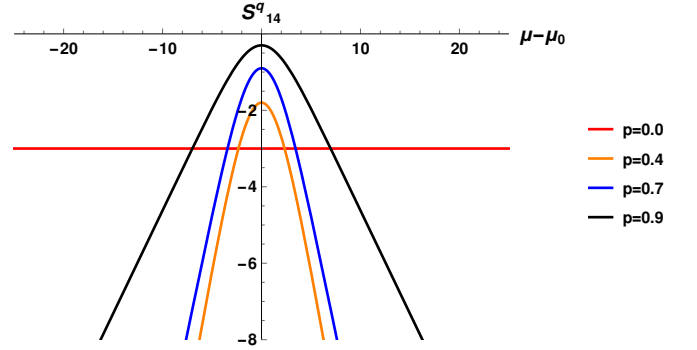


FIG. 6: Quantum noise S_{14}^q in units of $\frac{2e^2}{h} k_B \mathcal{T}$ for setup 1 as a function of $(\mu - \mu_0)$ in units of $k_B \mathcal{T}$ at $\mu_0 = 100k_B \mathcal{T}$ and $R = 0.5$.

Using Eq. (86), the distinction between the topological and trivial helical edge modes can be determined, as shown in Fig. 6. For topological helical edge modes ($p = 0$), the quantum noise is constant. In contrast, quantum noise for trivial helical edge modes with different spin-flip probabilities changes symmetrically with respect to the applied voltage ($eV = \mu - \mu_0$).

Similarly, other quantum noise cross-correlations are calculated. They are

$$S_{12}^q = S_{34}^q = -\frac{2e^2}{h} (1 - R) (1 - p) \left(2k_B \mathcal{T} + p \left[(\mu - \mu_0) \coth \left[\frac{\mu - \mu_0}{2k_B \mathcal{T}} \right] - 2k_B \mathcal{T} \right] \right). \quad (87)$$

Eq. (87) also distinguishes between the topological and trivial helical edge modes, shown in Fig. 7.

Similarly, we can calculate the quantum noise correlation between terminals 1, 3. We had already seen that the total contribution to this correlation comes from shot noise only. The equilibrium-like contribution is zero. So, in the trivial case, the actual contribution comes only

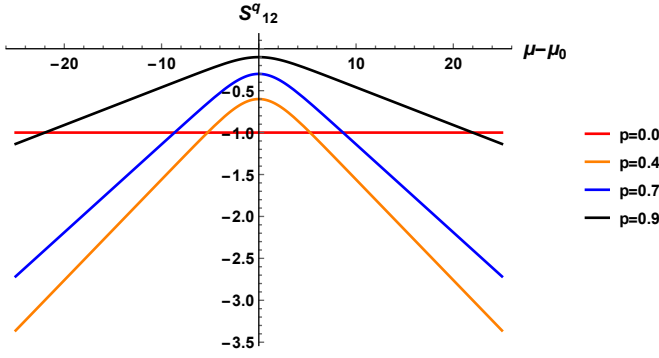


FIG. 7: Behaviour of quantum noise S_{12}^q in units of $\frac{2e^2}{h}k_B\mathcal{T}$ for setup 1 as a function of $(\mu - \mu_0)$ in units of $k_B\mathcal{T}$ at $\mu_0 = 100k_B\mathcal{T}$ and $R = 0.5$. S_{34}^q gives equally similar results too.

from shot noise. The shot noise-like contribution to S_{13}^q reduces the correlation for higher spin-flip scattering.

$$S_{13}^q = S_{13}^{sh} = -\frac{2e^2}{h}(1-p)^2R(1-R). \quad (88)$$

Similar to S_{13}^q , we see only the shot noise-like contribu-

$$\begin{aligned} S_{11}^q = S_{33}^q = & \frac{2e^2}{h} \left(4(1-p) + (1-R)(1-p) \left(\frac{\mu_0}{k_B\mathcal{T}} - \frac{\mu}{k_B\mathcal{T}} \right) + (1-p^2) \left(-1 + \frac{\mu}{k_B\mathcal{T}} \right) \right. \\ & \left. - (2p(1-p)(1-R) + 2(1-p)^2R(1-R)) \left(\frac{\exp\left(\frac{\mu}{k_B\mathcal{T}}\right) \frac{\mu_0}{k_B\mathcal{T}} - \exp\left(\frac{\mu_0}{k_B\mathcal{T}}\right) \frac{\mu}{k_B\mathcal{T}}}{\exp\left(\frac{\mu}{k_B\mathcal{T}}\right) - \exp\left(\frac{\mu_0}{k_B\mathcal{T}}\right)} \right) \right) \\ & - (1-p)^2(1-R)^2 \left(-1 + \frac{\mu_0}{k_B\mathcal{T}} \right) - 2p(1-p)R \left(-1 + \frac{\mu}{k_B\mathcal{T}} \right) - (1-p)^2R^2 \left(-1 + \frac{\mu}{k_B\mathcal{T}} \right) \Big) k_B\mathcal{T}. \end{aligned} \quad (91)$$

Similarly, the quantum noise autocorrelation in terminals 2 or 4 are the same; it can be seen by exchanging μ and μ_0 in S_{11}^q . The quantum noise autocorrelations $S_{11}^q, S_{22}^q, S_{33}^q, S_{44}^q$ changes symmetrically with the applied voltage ($eV = \mu - \mu_0$). We had already seen that for the topological helical case ($p = 0$), the quantum noise autocorrelation changes symmetrically with the applied voltage. In contrast, the autocorrelations for trivial helical edge modes change symmetrically for different values of spin-flip probability (p). Thus, for this setup, the trivial and topological helical edge modes are not distinguished via the quantum noise autocorrelation.

2. setup 2 [$\mu_1 = \mu_3 = \mu$ and $\mu_2 = \mu_4 = \mu_0$]

For this setup, we see that both quantum noise cross and autocorrelation can show the distinction between trivial and topological helical edge modes, and they are

tion to S_{24}^q is finite, and it is equal to S_{13}^q . The quantum noise correlation between terminals 2, 3 is always thermal noise-like.

The quantum noise autocorrelation in each terminal can also be found. The thermal noise contribution to the quantum noise autocorrelation in terminal 1 is,

$$S_{11}^{th} = \frac{2e^2}{h} \int_0^\infty dE (4(1-p)f(1-f)), \quad (89)$$

and the shot noise-like contribution is,

$$\begin{aligned} S_{11}^{sh} = & \frac{2e^2}{h} \int_0^\infty dE ((1-R)(1-p)(f_0 - f) \\ & + (1-p^2)f^2 - 2p(1-p)(1-R)ff_0 - (1-p)^2(1-R)^2f_0^2 \\ & - 2p(1-p)Rf^2 - 2(1-p)^2R(1-R)ff_0 - (1-p)^2R^2f^2), \end{aligned} \quad (90)$$

The quantum noise auto correlation in terminal 1 is $S_{11}^q = S_{11}^{th} + S_{11}^{sh}$. The quantum noise autocorrelation in terminal 3 is exactly the same as that of terminal 1 in the limit $\mu, \mu_0 \gg k_B\mathcal{T}$, which is given as,

given as,

$$\begin{aligned} S_{12}^q = S_{34}^q = & \frac{-2e^2}{h} (1-R)(1-p) \\ & \times \left(2k_B\mathcal{T} + p \left[(\mu - \mu_0) \coth \left[\frac{\mu - \mu_0}{2k_B\mathcal{T}} \right] - 2k_B\mathcal{T} \right] \right), \\ S_{14}^q = S_{23}^q = & \frac{-2e^2}{h} (1+R)(1-p) \\ & \times \left(2k_B\mathcal{T} + p \left[(\mu - \mu_0) \coth \left[\frac{\mu - \mu_0}{2k_B\mathcal{T}} \right] - 2k_B\mathcal{T} \right] \right), \quad (92) \\ S_{13}^q = & 0, \\ S_{24}^q = S_{24}^{sh} = & -\frac{2e^2}{h} 4R(1-R) \left[(\mu - \mu_0) \coth \left[\frac{(\mu - \mu_0)}{2k_B\mathcal{T}} \right] - 2k_B\mathcal{T} \right]. \end{aligned}$$

In Fig. 8, we see that for topological helical edge modes, S_{12}^q is constant since it is contributed by thermal

noise only. In contrast, for trivial helical edge modes, i.e., for non-zero spin-flip scattering values, it changes symmetrically with the applied voltage ($eV = \mu - \mu_0$). It effectively distinguishes between topological and trivial helical edge modes. Similar results are obtained for other quantum noise cross-correlations such as S_{14}^q and S_{23}^q shown in Fig. 9.

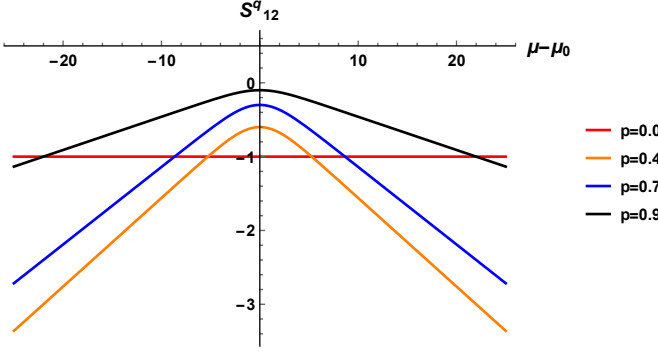


FIG. 8: Quantum noise S_{12}^q in units of $\frac{2e^2}{h}k_B\mathcal{T}$ for setup 2 as a function of $(\mu - \mu_0)$ in units of $k_B\mathcal{T}$ at $\mu_0 = 100k_B\mathcal{T}$ and $R = 0.5$. S_{34}^q gives equally similar results

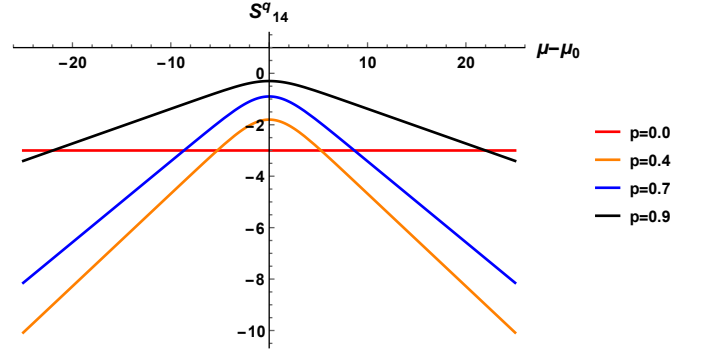


FIG. 9: Quantum noise S_{14}^q in units of $\frac{2e^2}{h}k_B\mathcal{T}$ for setup 2 as a function of $(\mu - \mu_0)$ in units of $k_B\mathcal{T}$ for $\mu_0 = 100k_B\mathcal{T}$ and $R = 0.5$. S_{23}^q gives similar results.

Similarly, the quantum noise autocorrelations can also be obtained. The thermal noise like contribution to S_{11}^q is,

$$S_{11}^{th} = \frac{2e^2}{h} \int_0^\infty dE (4(1-p)f(1-f)), \quad (93)$$

and the shot noise-like contribution is,

$$\begin{aligned} S_{11}^{sh} = & \frac{2e^2}{h} \int_0^\infty dE (2(1-p)(f_0 - f) + 2(1-p^2)f^2 \\ & - 2p(1-p)(1-R)ff_0 - (1-p)^2(1-R)^2f_0^2 \\ & - 2p(1-p)Rff_0 - 2(1-p)^2R(1-R)f_0^2 \\ & - (1-p)^2R^2f_0^2 - 2p(1-p)ff_0 - (1-p)^2f_0^2). \end{aligned} \quad (94)$$

The quantum noise autocorrelation in terminal 1 can be obtained by adding Eqs. (93) and (94), which is the same as that of terminal 3. The quantum noise autocorrelation in terminal 3 in the limit $\mu, \mu_0 \gg k_B\mathcal{T}$. The quantum noise autocorrelations S_{11}^q , which is equal to S_{33}^q is given by,

$$\begin{aligned} S_{11}^q = S_{33}^q = & \frac{2e^2}{h} \left(4(1-p) + 2(1-p) \left(\frac{\mu_0}{k_B\mathcal{T}} - \frac{\mu}{k_B\mathcal{T}} \right) + 2(1-p^2) \left(-1 + \frac{\mu}{k_B\mathcal{T}} \right) \right. \\ & \left. - (2p(1-p)(1-R) + 2p(1-p)R + 2p(1-p)) \left(\frac{\exp\left(\frac{\mu}{k_B\mathcal{T}}\right) \frac{\mu_0}{k_B\mathcal{T}} - \exp\left(\frac{\mu_0}{k_B\mathcal{T}}\right) \frac{\mu}{k_B\mathcal{T}}}{\exp\left(\frac{\mu}{k_B\mathcal{T}}\right) - \exp\left(\frac{\mu_0}{k_B\mathcal{T}}\right)} \right) \right. \\ & \left. + (-(1-p)^2(1-R)^2 - 2(1-p)^2R(1-R) - (1-p)^2R^2 - (1-p)^2) \left(-1 + \frac{\mu_0}{k_B\mathcal{T}} \right) \right) k_B\mathcal{T}. \end{aligned} \quad (95)$$

The quantum noise autocorrelation S_{22}^q , which is exactly equal to S_{44}^q in the limit $\mu, \mu_0 \gg k_B\mathcal{T}$, can be obtained by exchanging μ and μ_0 in S_{11}^q . Now, by taking $\mu_0 = 100k_B\mathcal{T}$ and $R = 0.5$, we can plot each quantum noise autocorrelations for different values of spin-flip scattering probability p . In the limit $\mu, \mu_0 \gg k_B\mathcal{T}$, each quantum noise autocorrelations is the same as shown in

Fig. 10.

3. setup 3 [$\mu_1 = \mu_2 = \mu$ and $\mu_3 = \mu_4 = \mu_0$]

In this setup, the difference between the topological and trivial helical edge modes can be shown via quantum

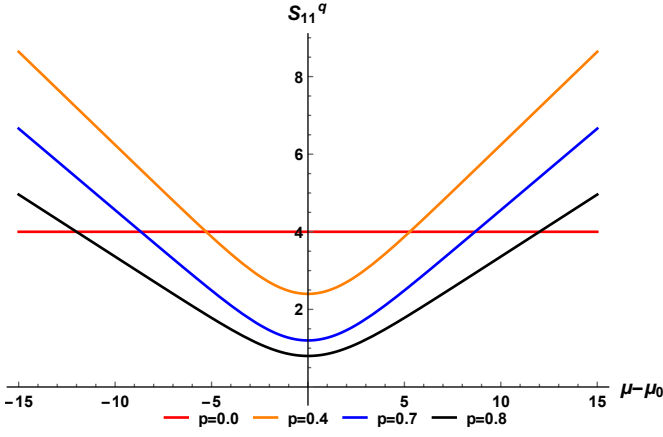


FIG. 10: Behaviour of autocorrelation quantum noise $S_{11}^q = S_{22}^q = S_{33}^q = S_{44}^q$ in units of $\frac{2e^2}{h}k_B\mathcal{T}$ for setup 2 as a function of applied voltage $(\mu - \mu_0)$ in units of $k_B\mathcal{T}$ with $R = 0.5$ and $\mu_0 = 100k_B\mathcal{T}$.

noise cross-correlations: S_{12}^q , S_{14}^q and S_{23}^q . The quantum noise correlation between different terminals is given as,

$$\begin{aligned}
 S_{12}^q &= -\frac{2e^2}{h}(1-R)(1-p)\left(2k_B\mathcal{T} + 4p\right. \\
 &\quad \left. \left[(\mu - \mu_0) \coth \left[\frac{(\mu - \mu_0)}{2k_B\mathcal{T}} \right] - 2k_B\mathcal{T} \right] \right), \\
 S_{14}^q = S_{23}^q &= -\frac{2e^2}{h}(1+R)(1-p)\left(2k_B\mathcal{T} + p\right. \\
 &\quad \left. \left[(\mu - \mu_0) \coth \left[\frac{(\mu - \mu_0)}{2k_B\mathcal{T}} \right] - 2k_B\mathcal{T} \right] \right), \quad (96) \\
 S_{34}^q &= -\frac{4e^2}{h}(1-R)(1-p)k_B\mathcal{T}, \\
 S_{13}^q = S_{24}^q = S_{13}^{sh} = S_{24}^{sh} &= -\frac{2e^2}{h}4R(1-R) \\
 &\quad \left[(\mu - \mu_0) \coth \left[\frac{(\mu - \mu_0)}{2k_B\mathcal{T}} \right] - 2k_B\mathcal{T} \right].
 \end{aligned}$$

Eq. (94) implies that the thermal noise contributions to $S_{12}^q, S_{14}^q, S_{23}^q, S_{13}^q, S_{24}^q$ are given as,

$$\begin{aligned}
 S_{12}^{th} &= \frac{2e^2}{h}(1-R)(1-p)2k_B\mathcal{T}, \\
 S_{14}^{th} = S_{23}^{th} &= \frac{(1+R)}{(1-R)}S_{12}^{th}, \quad (97) \\
 S_{13}^{th} = S_{24}^{th} &= 0.
 \end{aligned}$$

and the shot noise-like contributions are,

$$\begin{aligned}
 S_{12}^{sh} &= -\frac{2e^2}{h}(1-R)(1-p) \\
 &\quad \left(4p \left[(\mu - \mu_0) \coth \left[\frac{(\mu - \mu_0)}{2k_B\mathcal{T}} \right] - 2k_B\mathcal{T} \right] \right), \quad (98) \\
 S_{14}^{sh} = S_{23}^{sh} &= \frac{(1+R)}{4(1-R)}S_{12}^{sh}.
 \end{aligned}$$

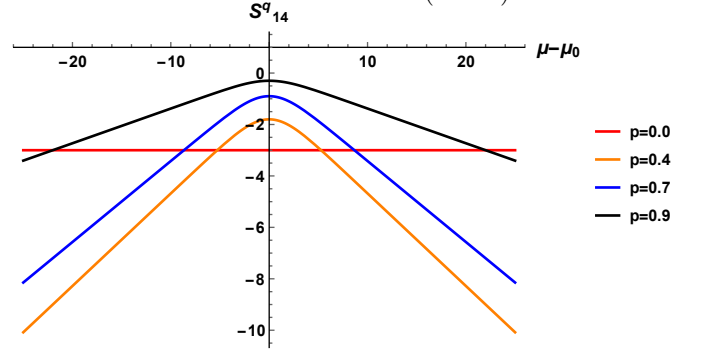


FIG. 11: Quantum noise $S_{14}^q = S_{23}^q$ in units of $\frac{2e^2}{h}k_B\mathcal{T}$ for setup 3 as a function of $(\mu - \mu_0)$ in units of $k_B\mathcal{T}$ with $\mu_0 = 100k_B\mathcal{T}$ and $R = 0.5$.

In this setup, the thermal noise-like contribution to S_{11}^q is,

$$S_{11}^{th} = S_{22}^{th} = \frac{2e^2}{h} \int_0^\infty 4(1-p)f(1-f), \quad (99)$$

and the shot noise-like contributions are,

$$\begin{aligned}
 S_{11}^{sh} &= \frac{2e^2}{h} \int_0^\infty \left((R+1)(1-p)(f_0 - f) + 2(1-p^2)f^2 \right. \\
 &\quad - 2p(1-p)(1-R)f^2 - (1-R)^2(1-p)^2f^2 \\
 &\quad - 2pR(1-p)ff_0 - 2R(1-R)(1-p)^2ff_0 \\
 &\quad - R^2(1-p)^2f_0^2 - (1-p)^2f_0^2 \\
 &\quad \left. - 2p(1-p)ff_0 \right), \quad (100)
 \end{aligned}$$

In the limit $\mu, \mu_0 \gg k_B\mathcal{T}$, the quantum noise auto-correlation S_{11}^q is exactly similar to S_{22}^q and is given as,

$$\begin{aligned}
S_{11}^q = S_{22}^q = & \frac{2e^2}{h} \left((R+1)(1-p) \left(\frac{\mu_0}{k_B\mathcal{T}} - \frac{\mu}{k_B\mathcal{T}} \right) + 2(1-p^2 - (2p(1-p)(1-R) + (1-R)^2(1-p)^2) \right. \\
& \left. \left(-1 + \frac{\mu}{k_B\mathcal{T}} \right) - (2pR(1-p) + 2R(1-R)(1-p)^2 + 2p(1-p)) \left(\frac{\exp\left(\frac{\mu}{k_B\mathcal{T}}\right) \frac{\mu_0}{k_B\mathcal{T}} - \exp\left(\frac{\mu_0}{k_B\mathcal{T}}\right) \frac{\mu}{k_B\mathcal{T}}}{\exp\left(\frac{\mu}{k_B\mathcal{T}}\right) - \exp\left(\frac{\mu_0}{k_B\mathcal{T}}\right)} \right) \right) \\
& - \left((R^2(1-p)^2 + (1-p)^2) \left(-1 + \frac{\mu_0}{k_B\mathcal{T}} \right) \right) k_B\mathcal{T}.
\end{aligned} \tag{101}$$

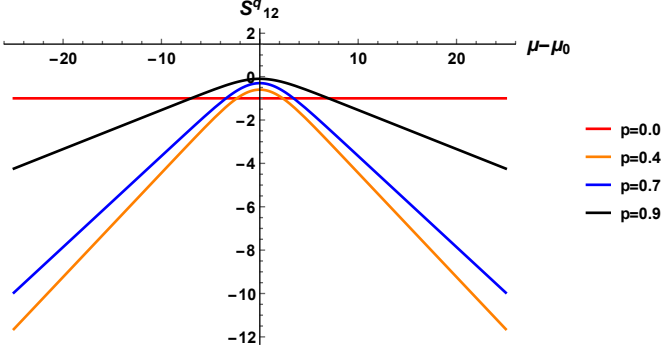


FIG. 12: Quantum noise S_{12}^q in units of $\frac{2e^2}{h}k_B\mathcal{T}$ for setup 3 as a function of $(\mu - \mu_0)$ in units of $k_B\mathcal{T}$ at $\mu_0 = 100k_B\mathcal{T}$ and $R = 0.5$.

The quantum noise autocorrelations S_{33}^q , which is exactly equal to S_{44}^q can be obtained by exchanging μ and μ_0 in S_{11}^q . Similar to setup 1, the quantum noise autocorrelations change symmetrically with applied voltage $eV = \mu - \mu_0$ for both the topological ($p = 0$) and trivial ($p \neq 0$) helical edge modes, which does not distinguish these two helical edge modes.

In setup 3, we observe that the topological and trivial helical edge modes are distinguished via the quantum noise correlations $S_{12}^q, S_{14}^q, S_{23}^q$ as shown in Fig. 11 and 12. Unlike setup 2, we do not see any instance where the quantum noise autocorrelation can discriminate between topological and trivial helical edge states.

IV. ANALYSIS

This section analyses all the possible cross and auto-quantum noise correlations for different setups via Tables I, II, and III.

In TABLE I, we have summarised the behaviour of all the possible cross and autocorrelations as a function of the voltage bias $(\mu - \mu_0)$ for setup 1 with the condition $\mu_1 = \mu_4 = \mu$ and $\mu_2 = \mu_3 = \mu_0$. We observe that

the quantum noise cross-correlations behave very similarly in the presence of chiral and helical edge modes except S_{24}^q , shown in Fig. 3. For chiral edge modes, it is zero. In contrast, in the presence of topological helical edge modes, shot noise-like contribution is finite, which gives nonvanishing quantum noise correlation S_{24}^q . Similarly, for setup 1, we see the distinction between trivial helical and topological helical edge modes via quantum noise correlation such as $S_{12}^q, S_{14}^q, S_{34}^q$, which are all constant for topological helical edge modes, while change while being symmetric with respect to the sign of voltage bias $(\mu - \mu_0)$ for trivial helical edge modes. It is shown in Figs. 6 and 7. Similarly, we have also looked into autocorrelations and summarised them in TABLE I. Chiral is distinguished from topological helical edge mode transport via the quantum noise autocorrelations S_{22}^q and S_{44}^q as in Fig. 4.

Similarly, quantum noise cross and autocorrelations for setup 2 with the condition $\mu_1 = \mu_3 = \mu$ and $\mu_2 = \mu_4 = \mu_0$ are summarised in TABLE II. We did not observe any examples of chiral and topological helical edge modes distinguished via quantum noise cross-correlation in this setup. Similar to setup 1, most of the examples clearly distinguish between the helical edge modes, trivial and topological, via the quantum noise cross-correlations $S_{12}^q, S_{14}^q, S_{23}^q, S_{34}^q$ as shown in Fig. 8 and 9. Here, autocorrelations do not discriminate between chiral and topological helical edge modes. However, they distinguish between topological and trivial helical edge modes, which can be seen in Fig. 10. The autocorrelations are constant due to topological helical edge modes and change symmetrically with respect to the change in sign of voltage bias for trivial helical.

For the third setup with the condition $\mu_1 = \mu_2 = \mu$ and $\mu_3 = \mu_4 = \mu_0$, the results are summarised in TABLE III. The distinction between chiral and topological helical is not seen for the cross-correlations of quantum noise. However, it is seen between topological and trivial helical edge modes for the quantum noise correlations $S_{12}^q, S_{14}^q, S_{23}^q$ as shown in Figs. 11 and 12. Similar to setup 1, the quantum noise autocorrelations S_{22}^q and S_{44}^q clearly distinguish between the chiral and topological helical edge modes.

V. EXPERIMENTAL REALIZATIONS AND CONCLUSION

Previously, there have been many attempts to distinguish trivial and topological helical edge modes by many

groups. In [8], it has already been pointed out that

TABLE I: Quantum noise cross and autocorrelation as a function of voltage bias($\mu - \mu_0$) for setup 1.

Edge Modes	$S_{12}^q = S_{34}^q$	S_{13}^q	S_{14}^q	S_{23}^q	S_{24}^q	$S_{11}^q = S_{33}^q$	$S_{22}^q = S_{44}^q$
Chiral	Constant	Symmetric	Constant	Constant	Zero	Symmetric	Constant
Helical(Topological)	Constant	Symmetric	Constant	Constant	Symmetric	Symmetric	Symmetric
Helical(Trivial)	Symmetric	Symmetric	Symmetric	Constant	Symmetric	Symmetric	Symmetric

TABLE II: Quantum noise cross and autocorrelation as a function of voltage bias($\mu - \mu_0$) for setup 2.

Edge Modes	$S_{12}^q = S_{34}^q$	S_{13}^q	$S_{14}^q = S_{23}^q$	S_{24}^q	$S_{11}^q = S_{22}^q = S_{33}^q = S_{44}^q$
Chiral	Constant	Zero	Constant	Symmetric	Constant
Helical(Topological)	Constant	Zero	Constant	Symmetric	Constant
Helical(Trivial)	Symmetric	Zero	Symmetric	Symmetric	Symmetric

TABLE III: Quantum noise cross and autocorrelation as a function of voltage bias($\mu - \mu_0$) for setup 3.

Edge Modes	S_{12}^q	S_{13}^q	$S_{14}^q = S_{23}^q$	S_{24}^q	S_{34}^q	$S_{11}^q = S_{33}^q$	$S_{22}^q = S_{44}^q$
Chiral	Constant	Symmetric	Constant	Symmetric	Constant	Symmetric	Constant
Helical(Topological)	Constant	Symmetric	Constant	Symmetric	Constant	Symmetric	Symmetric
Helical(Trivial)	Symmetric	Symmetric	Symmetric	Symmetric	Constant	Symmetric	Symmetric

even if edge channel conduction in the trivial regime in InAs/GaSb is seen, distinguishing trivial from topological edge modes via the conductance measurement is a complex task. The measurements on conductance in trivial regime showed similar results predicted in topological helical edge modes, which did not help distinguish trivial from topological helical edge modes. In another work[11], tuning between trivial and topological phases is effected through electrical gating, and the discrimination between trivial and topological phases via Hall resistance and longitudinal resistance, but it requires a high magnetic and electric field. In that case, our work concerning the finite temperature quantum noise autocorrelation and cross-correlation provides a more in-depth analysis of chiral, topological, and trivial helical edge modes, which helps distinguish between the edge modes.

In this paper, we are in the regime $\mu - \mu_0 \gg k_B \mathcal{T}$, wherein shot noise dominates the thermal noise. Experiments on shot noise are generally done at low temperatures because at higher temperatures, thermal noise tends to dominate the shot noise, and analyzing the nature of edge modes would be impossible[15]. In most cases, shot noise only plays a vital role in distinguishing between different edge modes. Otherwise, the quantum noise remains constant due to the finite temperature.

This work has made an essential contribution to topological phases and edge states. By analyzing the finite temperature quantum noise cross-correlation and autocorrelation, we have been able to distinguish between different edge modes, such as chiral, topological, and trivial helical edge modes. The results, presented in Tables I, II, and III, provide valuable insights into the behaviour of these edge modes under different conditions and demonstrate the usefulness of noise correlations in distinguishing between topological and trivial edge modes. Our work has considered finite temperatures and a diversity of setups, which are critical factors in experimental studies.

The findings of our study have important implications for future research and may help guide the development of new experimental techniques. Soon we plan to extend our study to thermoelectric properties, which would also be an exciting area of research that could shed further light on the nature of topological and trivial edge modes.

ACKNOWLEDGMENTS

The grants supported this work, ‘‘Josephson junctions with strained Dirac materials and their application in quantum information processing,’’ from the Science and Engineering Research Board (SERB), New Delhi, Government of India, under Grant No. CRG/2019/006258.

Appendix A: Derivation of thermal noise-like contribution for chiral edge mode transport

The quantum noise correlation in the presence of chiral edge modes is

$$S_{\alpha\beta}^q = \frac{e^2}{2\pi\hbar} \sum_{\gamma,\delta} \int dE \text{Tr}[A_{\gamma\delta}(\alpha)] \quad (\text{A1})$$

$$A_{\delta\gamma}(\beta)](f_\gamma(E)[1 - f_\delta(E)] + [1 - f_\gamma(E)]f_\delta(E)),$$

If the system is in thermal equilibrium at temperature \mathcal{T} , the Fermi-Dirac distribution in all the terminals is equal (assuming the chemical potential in each terminal are same), and we denote it by $f(E)$. Now, the above expression reduces to

$$S_{\alpha\beta}^{th} = 2 \frac{e^2}{2\pi\hbar} \int dE f(E)[1 - f(E)] \times \sum_{\gamma,\delta} \text{Tr}[A_{\gamma\delta}(\alpha)A_{\delta\gamma}(\beta)] \quad (\text{A2})$$

Now, using the formula for the matrix $A_{\beta\gamma}(\alpha)$, we get the expression to be

$$S_{\alpha\beta}^{th} = 2 \frac{e^2}{2\pi\hbar} \int dE f(E) [1 - f(E)] \times \sum_{\gamma,\delta} Tr[(\delta_{\alpha\gamma}\delta_{\alpha\delta} - s_{\alpha\gamma}^\dagger s_{\alpha\delta})(\delta_{\beta\delta}\delta_{\beta\gamma} - s_{\beta\delta}^\dagger s_{\beta\gamma})] \quad (A3)$$

Looking at the middle expression, we get

$$A_{\gamma\delta}(\alpha)A_{\delta\gamma}(\beta) = (I_\alpha\delta_{\alpha\gamma}\delta_{\alpha\delta}\delta_{\beta\gamma}\delta_{\beta\delta} - \delta_{\beta\gamma}\delta_{\beta\delta}s_{\alpha\gamma}^\dagger s_{\alpha\delta} - \delta_{\alpha\gamma}\delta_{\alpha\delta}s_{\beta\delta}^\dagger s_{\beta\gamma} + s_{\alpha\gamma}^\dagger s_{\alpha\delta}s_{\beta\delta}^\dagger s_{\beta\gamma}) \quad (A4)$$

Now, considering the summation over γ , we get

$$Tr[A_{\gamma\delta}(\alpha)A_{\delta\gamma}(\beta)] = Tr[I_\alpha\delta_{\alpha\delta}\delta_{\beta\alpha}\delta_{\beta\delta} - \delta_{\beta\delta}s_{\alpha\beta}^\dagger s_{\alpha\delta} - \delta_{\alpha\delta}s_{\beta\delta}^\dagger s_{\beta\alpha} + I_\alpha\delta_{\alpha\beta}s_{\alpha\delta}s_{\beta\delta}^\dagger] \quad (A5)$$

Then the summation over δ is given by

$$Tr[A_{\gamma\delta}(\alpha)A_{\delta\gamma}(\beta)] = Tr[2I_\alpha\delta_{\beta\alpha} - s_{\alpha\beta}^\dagger s_{\alpha\beta} - s_{\beta\alpha}^\dagger s_{\beta\alpha}] \quad (A6)$$

The formula used above for the last term is

$$s_{\alpha\beta}^\dagger s_{\alpha\gamma} = I_\beta\delta_{\beta\gamma}$$

So, the equation (A2) is given by

$$S_{\alpha\beta}^{th} = \frac{e^2}{\pi\hbar} \int dE f(E) [1 - f(E)] \times Tr[2I_\alpha\delta_{\beta\alpha} - s_{\alpha\beta}^\dagger s_{\alpha\beta} - s_{\beta\alpha}^\dagger s_{\beta\alpha}] \quad (A7)$$

$$S_{\alpha\beta}^{th} = \frac{e^2}{\pi\hbar} \int dE f(E) [1 - f(E)] \times [2N_\alpha\delta_{\alpha\beta} - Tr(s_{\alpha\beta}^\dagger s_{\alpha\beta} - s_{\beta\alpha}^\dagger s_{\beta\alpha})] \quad (A8)$$

This equation is the *Nyquist – Johnson* noise. It is a result of thermal fluctuations.

For the case $\alpha = \beta$, we see the local correlation(thermal noise like) to be

$$S_{\alpha\alpha}^{th} = 4 \frac{e^2}{h} \int dE (f(E)(1 - f(E))) \times [N_\alpha - R_{\alpha\alpha}], \quad (A9)$$

$R_{\alpha\alpha}$ is the reflection probability for an electron to reflect from terminal α .

For $\alpha \neq \beta$, we see that the thermal noise-like contribution to quantum noise cross-correlation is

$$S_{\alpha\beta}^{th} = \frac{e^2}{\pi\hbar} \int dE (f(E)(1 - f(E))) \times -(T_{\alpha\beta} + T_{\beta\alpha}) \quad (A10)$$

Here, we have assumed the contacts were connected to the reservoirs with the same chemical potential. For a

general case, where the distribution function at terminals α and β is different, we can write

$$S_{\alpha\beta}^{th} = -\frac{2e^2}{h} \int dE [T_{\alpha\beta}f_\beta(1-f_\beta) + T_{\beta\alpha}f_\alpha(1-f_\alpha)] \quad (A11)$$

Where f_β and f_α are Fermi-Dirac distribution of contacts β and α .

Appendix B: Derivation of shot noise-like contribution in chiral edge modes

To derive the expression for shot noise, we have to subtract the thermal noise-like contribution from the quantum noise-like contribution. We denote the correlation due to shot noise as $S_{\alpha\beta}^{sh}$. The autocorrelation shot noise is

$$S_{\alpha\alpha}^{sh} = S_{\alpha\alpha}^q - S_{\alpha\alpha}^{th} \quad (B1)$$

We will use the formula

$$\sum_{\delta} f_{\delta} \left(\sum_{\gamma} Tr[A_{\gamma\delta}(\alpha)A_{\delta\gamma}(\beta)] \right) = Tr[I_\alpha - 2s_{\alpha\alpha}^\dagger s_{\alpha\alpha}]f_\alpha + \sum_{\alpha} Tr(s_{\alpha\delta}s_{\alpha\delta}^\dagger)f_\delta \quad (B2)$$

After doing the algebra, we find the quantity $S_{\alpha\alpha}^{sh}$ to be

$$S_{\alpha\alpha}^{sh} = \frac{2e^2}{h} \int dE \left(\sum_{\gamma} T_{\alpha\gamma}(f_\gamma - f_\alpha) + M_\alpha f_\alpha^2 - \sum_{\gamma\delta} Tr(s_{\alpha\gamma}s_{\alpha\delta}s_{\alpha\delta}^\dagger s_{\alpha\gamma}) \right). \quad (B3)$$

For the cross-correlation case $\alpha \neq \beta$, the shot noise like contribution

$$S_{\alpha\beta}^{sh} = S_{\alpha\beta}^q - S_{\alpha\beta}^{th} \quad (B4)$$

Using the formula

$$\sum_{\delta} f_{\delta} \left(\sum_{\gamma} Tr[A_{\gamma\delta}(\alpha)A_{\delta\gamma}(\beta)] \right) = -T_{\alpha\beta}f_\beta - T_{\beta\alpha}f_\alpha, \quad (B5)$$

and

$$\sum_{\gamma} f_{\gamma} \left(\sum_{\delta} Tr[A_{\gamma\delta}(\alpha)A_{\delta\gamma}(\beta)] \right) = -Tr(s_{\alpha\beta}^\dagger s_{\alpha\beta})f_\beta - Tr(s_{\beta\alpha}^\dagger s_{\beta\alpha})f_\alpha \quad (B6)$$

Subtracting Eq. (A10) from Eq. (A1), we get the shot noise-like contribution to be

$$S_{\alpha\beta}^{sh} = -2 \frac{e^2}{h} \int dE \sum_{\gamma,\delta} f_{\gamma} f_{\delta} Tr(s_{\alpha\gamma}^\dagger s_{\alpha\delta}s_{\beta\delta}^\dagger s_{\beta\gamma}) \quad (B7)$$

Now, using the linearity property of the trace ($\text{tr}(bA)=b\text{tr}(A)$), we get

$$S_{\alpha\beta}^{sh} = -2\frac{e^2}{h} \int dE \quad \text{Tr} \left[\left(\sum_{\gamma} f_{\gamma} s_{\beta\gamma}^{\dagger} s_{\alpha\gamma} \right) \times \left(\sum_{\delta} f_{\delta} s_{\alpha\delta} s_{\beta\delta}^{\dagger} \right) \right] \quad (\text{B8})$$

Since the s-matrix is unitary, each sum in the above equation will be zero. Therefore in the above equation, we replace the functions f_{γ} and f_{δ} by $f_{\gamma} - f_a$ and $f_{\delta} - f_b$, where f_a and f_b are any energy-dependent functions which make the shot noise non-zero.

So, the final correct expression for the shot noise is

$$S_{\alpha\beta}^{sh} = -2\frac{e^2}{h} \int dE \sum_{\gamma,\delta} (f_{\gamma} - f_a)(f_{\delta} - f_b) \text{Tr}(s_{\alpha\gamma}^{\dagger} s_{\alpha\delta} s_{\beta\delta}^{\dagger} s_{\beta\gamma}) \quad (\text{B9})$$

Appendix C: Derivation of thermal noise contribution in helical edge modes

The spin-polarised components of the quantum noise in the presence of helical edge modes are

$$S_{\alpha\alpha}^{\sigma\sigma'q} = \frac{e^2}{2\pi\hbar} \sum_{\rho,\rho'=\uparrow,\downarrow} \sum_{\gamma,\delta} \int dE \quad \text{Tr}[A_{\gamma\delta}^{\rho\rho'}(\alpha,\sigma)A_{\delta\gamma}^{\rho'\rho}(\alpha,\sigma')] (f_{\gamma}(E)[1 - f_{\delta}(E)] + [1 - f_{\gamma}(E)]f_{\delta}(E)), \quad (\text{C1})$$

The quantum noise expression if the Fermi-Dirac distribution in all the terminals are same comes only from thermal noise contribution, which is given by

$$S_{\alpha\beta}^{\sigma\sigma'th} = 2\frac{e^2}{2\pi\hbar} \int dE f(E)[1 - f(E)] \sum_{\gamma,\delta} \sum_{\rho,\rho'} \text{Tr}[A_{\gamma\delta}^{\rho\rho'}(\alpha,\sigma)A_{\delta\gamma}^{\rho'\rho}(\beta,\sigma')] \quad (\text{C2})$$

We proceed further using the expression for $A_{\gamma\delta}^{\rho\rho'}(\alpha,\sigma)$ and we get,

$$S_{\alpha\beta}^{\sigma\sigma'th} = 2\frac{e^2}{2\pi\hbar} \int dE f(E)[1 - f(E)] \sum_{\gamma,\delta} \text{Tr}[(\delta_{\alpha\gamma}\delta_{\alpha\delta} - s_{\alpha\gamma}^{\sigma\rho\dagger} s_{\alpha\delta}^{\sigma\rho'}) (\delta_{\beta\delta}\delta_{\beta\gamma} - s_{\beta\delta}^{\sigma'\rho'\dagger} s_{\beta\gamma}^{\sigma'\rho'})] \quad (\text{C3})$$

Further, by simplifying the algebra as we did for the chiral case, we get

$$\text{Tr}[A_{\gamma\delta}^{\rho\rho'}(\alpha,\sigma)A_{\delta\gamma}^{\rho'\rho}(\beta,\sigma')] = [2N_{\alpha}\delta_{\beta\alpha}\delta_{\sigma\sigma'} - \text{Tr}(s_{\alpha\beta}^{\sigma\sigma'\dagger} s_{\alpha\beta}^{\sigma\sigma'}) - \text{Tr}(s_{\beta\alpha}^{\sigma\sigma'\dagger} s_{\beta\alpha}^{\sigma\sigma'})] \quad (\text{C4})$$

For $\alpha = \beta$, the thermal noise-like contribution is

$$S_{\alpha\alpha}^{\sigma\sigma'th} = \frac{4e^2}{h} \int dE f_{\alpha}(1 - f_{\alpha}) \sum_{\alpha \neq \beta} T_{\alpha\beta}^{\sigma\sigma'}. \quad (\text{C5})$$

For $\alpha \neq \beta$ and if the distribution function in terminals α and β are different, then we get,

$$S_{\alpha\beta}^{\sigma\sigma'th} = -\frac{2e^2}{h} \int dE [T_{\alpha\beta}^{\sigma\sigma'} f_{\beta}(1 - f_{\beta}) + T_{\beta\alpha} f_{\alpha}(1 - f_{\alpha})] \quad (\text{C6})$$

Appendix D: Derivation of shot noise-like contribution in helical edge modes

We need to subtract the thermal noise contribution from the quantum noise to derive the shot noise part. For the autocorrelation $\alpha = \beta$, we have to subtract Eq. (C4) from Eq. (C1). After doing some algebra, we get the shot noise-like contribution to be

$$S_{\alpha\alpha}^{\sigma\sigma'sh} = \frac{2e^2}{h} \int dE \left(\sum_{\gamma} T_{\alpha\gamma}^{\sigma\sigma'} (f_{\gamma} - f_{\alpha}) + M_{\alpha}\delta_{\sigma\sigma'} f_{\alpha}^2 - \sum_{\gamma\delta} \sum_{\rho\rho'=\uparrow,\downarrow} \text{Tr}(s_{\alpha\gamma}^{\sigma\rho\dagger} s_{\alpha\delta}^{\sigma\rho'} s_{\alpha\delta}^{\sigma'\rho'\dagger} s_{\alpha\gamma}^{\sigma'\rho}) \right). \quad (\text{D1})$$

For the cross correlation case $\alpha \neq \beta$, we find

$$S_{\alpha\beta}^{\sigma\sigma'sh} = S_{\alpha\beta}^{\sigma\sigma'q} - S_{\alpha\beta}^{\sigma\sigma'th} \quad (\text{D2})$$

We use the formula,

$$\sum_{\delta} f_{\delta} \left(\sum_{\gamma} \text{Tr}[A_{\gamma\delta}^{\rho\rho'}(\alpha,\sigma)A_{\delta\gamma}^{\rho'\rho}(\alpha,\sigma)] \right) = -T_{\alpha\beta}^{\sigma\sigma'} f_{\beta} - T_{\beta\alpha}^{\sigma\sigma'} f_{\alpha} \quad (\text{D3})$$

Similarly,

$$\sum_{\gamma} f_{\gamma} \left(\sum_{\delta} \text{Tr}[A_{\gamma\delta}^{\rho\rho'}(\alpha,\sigma)A_{\delta\gamma}^{\rho'\rho}(\alpha,\sigma)] \right) = -T_{\alpha\beta}^{\sigma\sigma'} f_{\beta} - T_{\beta\alpha}^{\sigma\sigma'} f_{\alpha} \quad (\text{D4})$$

Using Eq. (D2) and (D3) in Eq. (C1), we find that

$$S_{\alpha\beta}^{\sigma\sigma'sh} = -2\frac{e^2}{h} \int dE \sum_{\gamma,\delta} (f_{\gamma} - f_a)(f_{\delta} - f_b) \text{Tr}(s_{\alpha\gamma}^{\sigma\rho\dagger} s_{\alpha\delta}^{\sigma\rho'} s_{\beta\delta}^{\sigma'\rho'\dagger} s_{\beta\gamma}^{\sigma'\rho'}) \quad (\text{D5})$$

-
- [1] K. v. Klitzing, G. Dorda, and M. Pepper, New method for high-accuracy determination of the fine-structure constant based on quantized hall resistance, *Phys. Rev. Lett.* **45**, 494 (1980).
- [2] M. Büttiker, Absence of backscattering in the quantum hall effect in multiprobe conductors, *Phys. Rev. B* **38**, 9375 (1988).
- [3] S. Datta, *Electronic Transport in Mesoscopic Systems*, Cambridge Studies in Semiconductor Physics and Microelectronic Engineering (Cambridge University Press, 1995).
- [4] C. L. Kane and E. J. Mele, Quantum spin hall effect in graphene, *Phys. Rev. Lett.* **95**, 226801 (2005).
- [5] B. A. Bernevig, T. L. Hughes, and S.-C. Zhang, Quantum spin hall effect and topological phase transition in hgte quantum wells, *Science* **314**, 1757 (2006), <https://www.science.org/doi/pdf/10.1126/science.1133734>.
- [6] M. König, S. Wiedmann, C. Brüne, A. Roth, H. Buhmann, L. Molenkamp, X. Qi, and S. Zhang, Quantum spin hall insulator state in hgte quantum wells, *Science* **318**, 776770 (2007).
- [7] S.-Q. Shen, *Topological Insulators* (Springer Singapore, 2017).
- [8] F. Nichele, H. J. Suominen, M. Kjaergaard, C. M. Marcus, E. Sajadi, J. A. Folk, F. Qu, A. J. A. Beukman, F. K. de Vries, J. van Veen, S. Nadj-Perge, L. P. Kouwenhoven, B.-M. Nguyen, A. A. Kiselev, W. Yi, M. Sokolich, M. J. Manfra, E. M. Spanton, and K. A. Moler, Edge transport in the trivial phase of inas/gasb, *New Journal of Physics* **18**, 083005 (2016).
- [9] A. Mani and C. Benjamin, Probing helicity and the topological origins of helicity via non-local hanbury-brown and twiss correlations, *Scientific Reports* **7**, 10.1038/s41598-017-06820-w (2017).
- [10] Y. M. Blanter and M. Büttiker, Shot noise in mesoscopic conductors, *Physics Reports* **336**, 1 (2000).
- [11] F. Qu, A. J. A. Beukman, S. Nadj-Perge, M. Wimmer, B.-M. Nguyen, W. Yi, J. Thorp, M. Sokolich, A. A. Kiselev, M. J. Manfra, C. M. Marcus, and L. P. Kouwenhoven, Electric and magnetic tuning between the trivial and topological phases in inas/gasb double quantum wells, *Phys. Rev. Lett.* **115**, 036803 (2015).
- [12] M. Büttiker, Scattering theory of current and intensity noise correlations in conductors and wave guides, *Phys. Rev. B* **46**, 12485 (1992).
- [13] R. Landauer and T. Martin, Equilibrium and shot noise in mesoscopic systems, *Physica B: Condensed Matter* **175**, 167 (1991), analogies in Optics and Microelectronics.
- [14] R. L. Dragomirova and B. K. Nikolić, Shot noise of spin-polarized charge currents as a probe of spin coherence in spin-orbit coupled nanostructures, *Phys. Rev. B* **75**, 085328 (2007).
- [15] K. Kobayashi and M. Hashisaka, Shot noise in mesoscopic systems: From single particles to quantum liquids, *J. Phys. Soc. Jpn.* **90**, 1 (2021).
- [16] D. C. Tsui, H. L. Stormer, and A. C. Gossard, Two-dimensional magnetotransport in the extreme quantum limit, *Phys. Rev. Lett.* **48**, 1559 (1982).
- [17] A. Roth, C. Brüne, H. Buhmann, L. W. Molenkamp, J. Maciejko, X.-L. Qi, and S.-C. Zhang, Nonlocal transport in the quantum spin hall state, *Science* **325**, 294 (2009).
- [18] T. Mohapatra, S. Pal, and C. Benjamin, Probing the topological character of superconductors via nonlocal hanbury brown and twiss correlations, *Phys. Rev. B* **106**, 125402 (2022).
- [19] W. Chen, W.-Y. Deng, J.-M. Hou, D. N. Shi, L. Sheng, and D. Y. Xing, π spin berry phase in a quantum-spin-hall-insulator-based interferometer: Evidence for the helical spin texture of the edge states, *Phys. Rev. Lett.* **117**, 076802 (2016).
- [20] J. Eriksson, M. Acciai, L. Tesser, and J. Splettstoesser, General bounds on electronic shot noise in the absence of currents, *Phys. Rev. Lett.* **127**, 136801 (2021).